arXiv:cond-mat/0307509v1 [cond-mat.supr-con] 21 Jul 2003

C axis lattice dynamics in Bi-based cuprate superconductors

N.N. Kovaleva,* A.V. Boris,* T. Holden, C. Ulrich,

B. Liang, C.T. Lin, B. Keimer, and C. Bernhard

Max-Planck-Institut für Festkörperforschung,

Heisenbergstrasse 1, D-70569 Stuttgart, Germany

J.L. Tallon

McDiarmid Institute and Industrial Research Laboratory, Lower Hutt New-Zealand

D. Munzar

Institute of Condensed Matter Physics,

Faculty of Science, Masaryk University,

Kotlářská 2, CZ-61137 Brno, Czech Republic

A.M. Stoneham

University College London, London WC1E 6BT, United Kingdom

(Dated: March 22, 2022)

Abstract

We present results of a systematic study of the c axis lattice dynamics in single layer $Bi_2Sr_2CuO_6$ (Bi2201), bilayer $Bi_2Sr_2CaCu_2O_8$ (Bi2212) and trilayer $Bi_2Sr_2Ca_2Cu_3O_{10}$ (Bi2223) cuprate superconductors. Our study is based on both experimental data obtained by spectral ellipsometry on single crystals and theoretical calculations. The calculations are carried out within the framework of a classical shell model, which includes long-range Coulomb interactions and short-range interactions of the Buckingham form in a system of polarizable ions. Using the same set of the shell model parameters for Bi2201, Bi2212 and Bi2223, we calculate the frequencies of the Brillouin-zone center phonon modes of A_{2u} symmetry and suggest the phonon mode eigenvector patterns. We achieve good agreement between the calculated A_{2u} eigenfrequencies and the experimental values of the c axis TO phonon frequencies which allows us to make a reliable phonon mode assignment for all three Bi-based cuprate superconductors. We also present the results of our shell model calculations for the Γ-point A_{1g} symmetry modes in Bi2201, Bi2212 and Bi2223 and suggest an assignment that is based on the published experimental Raman spectra. The superconductivity-induced phonon anomalies recently observed in the c axis infrared and resonant Raman scattering spectra in trilayer Bi2223 are consistently explained with the suggested assignment.

PACS numbers: 74.72.Hs, 74.25Kc, 78.20.Bh, 63.20.Dj

*Also at the Institute for Solid State Physics, Russian Academy of Sciences, Chernogolovka, Moscow distr., 142432 Russia

I. INTRODUCTION

The unusual c axis charge transport in the cuprate high-T_c superconductors is still a subject of a controversial discussion. Of particular interest is a sizable absorption peak that develops below T_c in the far-infrared (FIR) range, accompanied with the strongly anomalous temperature dependence of some of the c-polarized IR phonon modes, in compounds that contain more than one CuO_2 plane per unit cell. Recently a reasonable description of these effects has been obtained with the so-called Josephson-superlattice model [1, 2, 3, 4, 5, 6]. Here it is assumed that the individual CuO_2 planes are only weakly coupled by Josephson currents in the superconducting state. For bilayer compounds like $YBa_2Cu_3O_{7-\delta}$ (Y123) and $Bi_2Sr_2CaCu_2O_8$ (Bi2212) this results in two kinds of Josephson junctions with different longitudinal plasma frequencies, and their out-of-phase oscillation gives rise to a transverse Josephson plasma resonance, which has been assigned to the absorption peak that develops below T_c; the Josephson currents lead to a modification of the dynamical local electric fields and thus are at the heart of the observed phonon anomalies [2, 4, 5, 6]. The trilayer compounds provide an interesting testing ground for the various models that have been put forward to explain the unusual c axis charge dynamics and the anomalous temperature dependence of some of the IR-active c-polarized phonon modes such as observed in the bilayer compounds. Indeed, very recent experimental study of the c axis optical conductivity of a trilayer $Bi_2Sr_2Ca_2Cu_3O_{10}$ (Bi2223) provides clear evidence that the transverse Josephson plasma resonance is a universal feature of the multilayer high-T_c cuprate compounds [7]. It has been shown that the Josephson-superlattice model [2, 4, 5, 6] allows qualitative description of the transverse Josephson plasma resonance and related phonon anomalies in Bi2223, which suggest that the Josephson currents lead to a strong variation of the dynamical local electric field even between the inner and the outer CuO_2 planes of a trilayer.

The assignment of the IR-active c-polarized phonon modes and their polarization diagrams are of great importance for understanding these phenomena. While the properties of the IR-active phonon modes are indeed well known for the Y123 system [8, 9, 10, 11], the situation is not that clear for the bilayer high-T_c compounds of the type $A_2Sr_2CaCu_2O_8$ (A2212; A = Tl, Bi). Despite of experimental [5, 6, 12, 13] and theoretical [14, 15, 16] efforts, the assignment of the c axis IR phonon modes in Bi2212 and Tl2212 remains contradictory, as discussed in [13]. The situation is even less satisfactory for the trilayer high-T_c compounds

$A_2Sr_2Ca_2Cu_3O_{10}$ (A2223) where the lack of single crystals of sufficient size and quality has inhibited detailed experimental investigations. Shell model calculations have been carried out for Tl2223 [17] and IR measurements have been performed on ceramic samples of Tl2223 [18] and more recently on oriented ceramics of Bi2223 [19]. The situation has changed only very recently when some of the present authors managed to grow high quality single crystals of the trilayer Bi-compound $Bi_2Sr_2Ca_2Cu_3O_{10}$ that are suitable for IR measurements with the light polarization along the c axis direction [20].

This manuscript reports a systematic investigation of the c axis lattice dynamics of the bismuth-based compounds $Bi_2Sr_2Ca_{n-1}Cu_nO_{2n+4+d}$ that contain either n = 1, 2, or 3 CuO_2 layers per unit cell. Our approach combines theoretical shell model based calculations with ellipsometric measurements of the c axis dielectric response on well characterized single crystals of high quality [20, 21, 22]. From the ellipsometry experiments we obtain the frequencies of the c axis polarized IR-active phonon modes as well as the dielectric constants. On the theoretical side we model the Bi-based compounds with n = 1, 2, and 3 in the *I4/mmm* space group using the shell model approach suggesting that screening due to free charge carriers should not have major effects [23]. This approach has been successfully applied to study lattice dynamics and various physical properties of high-T_c superconductors [14, 17, 24, 25]. The calculations have been performed using the GULP code [26]. The shell model parameters have been derived by fitting to the crystal structures in equilibrium as well as to experimental values of the dielectric constants and frequencies of the transverse optical (TO) phonon modes. Using the same set of shell model parameter for the n = 1, 2, and 3 compounds we calculate the eigenfrequencies of the Brillouin-zone center phonon modes of A_{2u} symmetry and derive the phonon mode eigenvector patterns. Our results for the bilayer compound Bi2212 are consistent with those of the earlier shell model calculations in the *I4/mmm* space group by Prade *et al.* [14]. We make an assignment of the c axis polarized phonon modes observed in the ellipsometric spectra of single, bi-, and trilayer Bi-based compounds by comparing with the calculated eigenfrequencies of A_{2u} symmetry modes. In addition, we also show the displacement patterns and calculated eigenfrequencies for the Raman-active phonon modes of A_{1g} symmetry according to the results of the present shell model calculations.

II. CRYSTAL STRUCTURE AND Γ-POINT PHONONS IN $Bi_2Sr_2Ca_{n-1}Cu_nO_{2n+4+\delta}$ WITH N = 1, 2 AND 3

As a first approximation, a body-centered-tetragonal structure ($I4/mmm$) has been most frequently used in the interpretation of the IR and Raman spectra of Tl- and Bi-based compounds. According to the x-ray data [27, 28], the three Bi-based cuprates of general formula $Bi_2Sr_2Ca_{n-1}Cu_nO_{2n+4+\delta}$ with n = 1, 2 and 3 have similar structures of the tetragonal $I4/mmm$ space group (a_{tetr} = 3.814 Å), with two formula units (two primitive unit cells) in the crystallographic cell, as illustrated in Figure 1. Primitive unit cells of single, bi- and trilayer Bi-based cuprates differ only in the number (n-1) of CuO_2-Ca-CuO_2 slabs packed along the c axis; upon insertion of one and two slabs the c axis parameter of the crystallographic cells increases from 24.6 to 30.6, and 37.1 Å [28]. The Wyckoff positions of the atoms and their site symmetries in tetragonal $I4/mmm$ (D_{4h}^{17}) primitive unit cells of $Bi_2Sr_2CuO_6$ (Bi2201), $Bi_2Sr_2CaCu_2O_8$ (Bi2212), and $Bi_2Sr_2Ca_2Cu_3O_{10}$ (Bi2223) are listed in Table 1, with the notations of the atoms given in Figure 2.

The irreducible representations corresponding to various atomic sites in the three Bi-based compounds that follow from the character tables of the point groups are presented in the right column of Table 1. For the IR-active modes at the Γ-point of the Brillouin zone the displacement symmetries are A_{2u} for a displacement in the z direction and E_u for displacements in the x or y directions, whereas those for the Raman-active Γ modes are A_{1g}, B_{1g} and E_g, respectively. Due to full point-group symmetry of the Cu1 (Bi2201), Cu2 (Bi2223) and Ca (Bi2212) atoms with the (1a) site position, no Raman-active modes of these atoms are allowed, and the three displacement vectors yield three modes of A_{2u} and E_u (doubly degenerate) character. The oxygen atoms in the mirror cuprate planes, O1 in single layer and O4 in trilayer Bi-compounds, of D_{2h} site symmetry, yield eigenmodes $A_{2u} + B_{2u} + 2E_u$. The in-plane oxygen O1 with C_{2v} site symmetry in the bilayer and trilayer compounds generates eigenmodes $A_{2u} + A_{1g} + B_{1g} + B_{2u} + 2E_g + 2E_u$, among them the B_{2u} mode is silent and E_g is doubly degenerated. The total numbers of modes grouped according to their optical activity in the three Bi-based compounds are summarized in Table 2.

It has been shown that the actual structure of Bi-based compounds is better represented by orthorhombic *Cccm* (D_{2h}^{20}) [29, 30, 31, 32] or *Ccc2* (C_{2v}^{13})) [33, 34] space groups, most of the structural studies verify that the orthorhombic *Cccm* structure is correct. To follow the

TABLE I: The irreducible representations for the atoms in tetragonal *I4/mmm* (D_{4h}^{17}) $Bi_2Sr_2CuO_6$ (Bi2201), $Bi_2Sr_2CaCu_2O_8$ (Bi2212) and $Bi_2Sr_2Ca_2Cu_3O_{10}$ (Bi2223).

Comp.	Atom	Wyc. not.	Site sym.	Irreducible	representation
Bi2201	Cu1	(1a)	D_{4h}	A_{2u}	$+ E_u$
	Bi, Sr, O2, O3	(2e)	C_{4v}	$4(A_{2u} + A_{1g}$	$+ E_g + E_u)$
	O1	(2c)	D_{2h}	A_{2u}	$+ B_{2u} + 2E_u$
Bi2212	Ca	(1a)	D_{4h}	A_{2u}	$+ E_u$
	Bi, Sr, Cu1, O2, O3	(2e)	C_{4v}	$5(A_{2u} + A_{1g}$	$+ E_g + E_u)$
	O1	(4g)	$C^v{}_{2v}$	$A_{2u} + A_{1g} + B_{1g}$	$+ B_{2u} + 2E_g + 2E_u$
Bi2223	Cu2	(1a)	D_{4h}	A_{2u}	$+ E_u$
	O4	(2c)	D_{2h}	A_{2u}	$+ B_{2u} + 2E_u$
	Bi, Sr, Ca, Cu1, O2, O3	(2e)	C_{4v}	$6(A_{2u} + A_{1g}$	$+ E_g + E_u)$
	O1	(4g)	$C^v{}_{2v}$	$A_{2u} + A_{1g} + B_{1g}$	$+ B_{2u} + 2E_g + 2E_u$

TABLE II: Modes classification from the irreducible representations for Bi2201, Bi2212 and Bi2223 in tetragonal *I4/mmm* (D_{4h}^{17}) space group.

Comp.	Γ_{IR}	Γ_{Raman}	$\Gamma_{acoustic}$	Γ_{silent}
Bi2201	$5A_{2u} + 6E_u$	$4A_{1g} + 4E_g$	$A_{2u} + E_u$	B_{2u}
Bi2212	$6A_{2u} + 7E_u$	$6A_{1g} + 7E_g + B_{1g}$	$A_{2u} + E_u$	B_{2u}
Bi2223	$8A_{2u} + 10E_u$	$7A_{1g} + 8E_g + B_{1g}$	$A_{2u} + E_u$	$2B_{2u}$

consequences of the lowering symmetry it is convenient to use the *Amaa* space group, which is a nonconventional setting of *Cccm*. The orthorhombic *Amaa* structure has two formula units per primitive face centered cell, with in-plane lattice parameters a and b of approximately $a_{tetr}\sqrt{2}$, and four formula units for crystallographic cell, with the same c axis parameter. By way of example, in the right column of Table 3 we present the irreducible representations corresponding to various atomic sites in the orthorhombic *Amaa* $Bi_4Sr_4Cu_2O_{12}$ (Bi2201) and $Bi_4Sr_4Ca_2Cu_4O_{16}$ (Bi2212) according to the structural data of Imai *et al.* [29], where we also show the modes which are silent in the tetragonal symmetry. The total numbers

TABLE III: The irreducible representations for the atoms in orthorhombic *Amaa* (D_{2h}^{20}) $Bi_4Sr_4Cu_2O_{12}$ (Bi2201)and $Bi_4Sr_4Ca_2Cu_4O_{16}$ (Bi2212).

Comp.	Atom	Wyc. not.	Irreducible representations
Bi2201	Cu1	(2e)	$A_u + 2B_{1u} + 2B_{2u} + B_{3u}$
			$B_{1u} + B_{2u}$ tetragonal silent
	Bi, Sr, O2, O3	(4l)	$4(A_u + 2B_{1u} + 2B_{2u} + B_{3u} + 2A_g + B_{1g} + B_{2g} + 2B_{3g})$
			$4(B_{1u} + B_{2u} + A_g + B_{1g} + B_{3g})$ tetragonal silent
	O1	(4h)	$A_u + B_{1u} + 2B_{2u} + 2B_{3u} + A_g + B_{1g} + 2B_{2g} + 2B_{3g}$
			$A_g + B_{1g} + 2B_{2g} + 2B_{3g}$ tetragonal silent
Bi2212	Ca	(2e)	$A_u + 2B_{1u} + 2B_{2u} + B_{3u}$
			$B_{1u} + B_{2u}$ tetragonal silent
	Bi, Sr, Cu1, O2, O3	(4l)	$5(A_u + 2B_{1u} + 2B_{2u} + B_{3u} + 2A_g + B_{1g} + B_{2g} + 2B_{3g})$
			$5(B_{1u} + B_{2u} + A_g + B_{1g} + B_{3g})$ tetragonal silent
	O11,O12	(4h)	$2(A_u + B_{1u} + 2B_{2u} + 2B_{3u} + A_g + B_{1g} + 2B_{2g} + 2B_{3g})$
			$B_{1u} + 2B_{2u} + 2B_{3u} + A_g + B_{1g} + 2B_{2g} + 2B_{3g}$ tetragonal silent

of modes grouped according to their optical activity in the *Amaa* Bi2201 and Bi2212 are summarized in Table 4. In Table 5 we show components of the IR and Raman-active normal modes of the atoms with different Wyckoff positions at the Γ-point of the Brillouin zone in the orthorhombic *Amaa* space group. From Tables 1 and 3 one can see that if the *I4/mmm* symmetry breaks down owing to the orthorhombic distortion of the structure, the degeneracy is removed. Thus, for each atom with (2e) site position in the *I4/mmm* symmetry (Bi, Sr, O2, O3 and Cu1 in Bi2212) normal modes A_{2u}, A_{1g}, one E_u, and one E_g will become nondegenerate and, as a result, split into two; in addition, one new mode of B_{1g} character will appear in the orthorhombic *Amaa* structure. For the atoms Cu1 in Bi2201 and Ca in Bi2212 two new IR-active modes of B_{1u} and B_{2u} character are expected in the *Amaa* structure. Due to breaking of the tetragonal symmetry the O1 atom in Bi2201 will become "Raman-active", and, as a result, a number of Raman-active modes of A_g, B_{1g}, $2B_{2g}$, and $2B_{3g}$ character will appear.

TABLE IV: Modes classification from the irreducible representations for Bi2201 and Bi2212 in orthorhombic *Amaa* space group.

Comp.	Γ_{IR}	Γ_{Raman}	$\Gamma_{acoustic}$	Γ_{silent}
Bi2201	$10B_{1u} + 11B_{2u} + 6B_{3u}$	$9A_g + 5B_{1g} + 6B_{2g} + 10B_{3g}$	$B_{1u} + B_{2u} + B_{3u}$	$6A_u$
Bi2212	$13B_{1u} + 15B_{2u} + 9B_{3u}$	$12A_g + 7B_{1g} + 9B_{2g} + 14B_{3g}$	$B_{1u} + B_{2u} + B_{3u}$	$8A_u$

TABLE V: Components of normal modes of atoms with different Wyckoff positions in orthorhombic *Amaa* space group.

Wyc. not.	A_g	A_u	B_{3g}	B_{3u}	B_{1g}	B_{1u}	B_{2g}	B_{2u}
(2e)		x		x		zy		yz
(4l)	zy	x	yz	x	x	zy	x	yz
(4h)	z	z	xy	xy	z	z	yx	yx

However, it has been known that the actual structure of Bi-based cuprates is only pseudo-orthorhombic due to stacking faults, extra-stoichiometric oxygen and incommensurate superstructural modulations along the b axis in BiO and SrO layers [35], which result in substantial oxygen and cation disorder. These factors can yield additional phonon modes, in particular, "disorder-induced" modes. The crystal structure of Bi-based compounds therefore should be described in terms of a larger elementary cell and lower crystal symmetry. The origin of the superstructural incommensurate modulations of the atoms in BiO and SrO layers is not fully understood. The most common assumption is that the modulations are associated with extra-stoichiometric oxygen in the bilayer $Bi_2O_{2+\delta}$ that affects the orthorhombicity in the Bi-based cuprates. In this situation, whatever approximation either tetragonal or orthorhombic is adopted to make an assignment in the experimental phonon spectra, the first problem one has to solve is to distinguish the extra phonon modes - beyond the considered symmetry - due to effects of superstructural incommensurate modulations and presence of extra-stoichiometric oxygen in the Bi-based compounds.

Since the deviation from tetragonality in Bi-based compounds is not large we suggest to start with the tetragonal $I4/mmm$ approximation assuming that modes silent in tetragonal symmetry will be weak, and the simple tetragonal $I4/mmm$ approximation should provide a useful first approximation for the assignment of the most intense IR and Raman-

active phonon modes. To explain more details in the experimental spectra due to possible orthorhombicity effects we suggest to invoke the group theory analysis based on the orthorhombic *Amaa* (D_{2h}^{20}) space group (see Table 3).

III. SAMPLES AND EXPERIMENTAL TECHNIQUE

The Bi2201, Bi2212 and Bi2223 single crystals have been grown by the travelling solvent floating zone (TSFZ) method [20, 21, 22]. The feed rods with the nominal composition of $Bi_{2.1}Sr_{1.9}Ca_{n-1}Cu_nO_{2n+4+\delta}$ (n = 1, 2 and 3) were prepared by the conventional solid state method. The slow growth rates of 0.5 and 0.2 mm/h were used for the Bi2201 and Bi2212 crystals, respectively. Since the Bi2223 crystallization field is the narrowest among the three members of Bi-based family, an extremely slow growth rate of 0.04 mm/h was used. The Bi2201, Bi2212 and Bi2223 crystals were grown under applied oxygen pressure $p(O_2)$, in air, and in mixed gas flow of 80% Ar and 20% O_2, respectively. Because of the significant difference between the lattice parameters of the a and b axis as compared to the one along the c axis, the growth rate is highly anisotropic and very slow along c. One typically obtains platelike crystals with large ab planes of about 6 $\times$2 mm^2 but with much smaller dimensions along the c axis. The typical thickness is 1.5 $\div$ 2 mm for Bi2201, about 1 mm for Bi2212, less than 1 mm for Bi2223.

The crystals were characterized by energy dispersive X-ray (EDX) analysis, X-ray diffraction (XRD), transmission electron microscopy (TEM), magnetic susceptibility and resistivity measurements. The as-grown Bi2212 crystals are phase-pure with a pseudotetragonal structure, they are almost optimally doped with T_c = 91 K and ΔT_c = 2 K. The as-grown Bi2223 crystal contains 95-98 % of the Bi2223 pseudotetragonal phase with a minor fraction of layer-intercallated Bi2212. In the as-grown state the Bi2223 crystal was underdoped with T_c = 97 K (midpoint) and ΔT_c (10-90% shielding fraction) = 7 K. After a post-annealing treatment for ten days in flowing oxygen at 500 °C with a subsequent rapid quenching to room temperature, the crystal became nearly optimally doped, with T_c = 107 K and ΔT_c = 3 K. The undoped Bi2201 crystals grown by the TSFZ method are often nonsuperconducting. The superconductivity of the as-grown Bi2201 crystals is critically controlled by the oxygen content, therefore the growth was carried out under oxygen pressures $p(O_2)$ ranging from 1 to 10 bar. The T_c of the as-grown Bi2201 crystals, determined from magnetic susceptibility

measurements varied between 3.5 and 8.5 K upon the Bi/Sr ratio and the oxygen pressure $p(O_2)$ applied in the course of growing. The structure of the as-grown Bi2201 crystals was determined to be pseudotetragonal, the lattice parameters were found to dependent upon the Bi/Sr ratio in the crystal composition. A pair of as-grown Bi2212 single crystals (taken from the same part of an ingot) was used for oxygen isotope replacement. The selected samples were annealed in isotopically enriched oxygen under identical conditions following a similar procedure described in Ref. [36].

For the ellipsometric measurements the crystal surfaces were polished to optical grade. The technique of ellipsometry provides significant advantages over conventional reflection methods in that (i) it is self-normalizing and does not require reference measurements and (ii) $\epsilon_1(\omega)$ and $\epsilon_2(\omega)$ are obtained directly without a Kramers-Kronig transformation (see Refs. [4, 37] for a description of the technique). The ellipsometric measurements have been performed at the U4IR beamline of the National Synchrotron Light Source (NSLS) at Brookhaven National Laboratory, USA and at the infrared beamline of the synchrotron radiation source ANKA at Karlsruhe Research Center, Germany. Home-built ellipsometers attached either to a Nicolet Magna 860 or a "Bruker" IFS 66v/S FT-IR spectrometer were used. The high brilliance of the synchrotron light source due to the small beam divergence enabled us to perform very accurate ellipsometric measurements in the far-IR range even on samples with comparably small *ac* faces.

IV. *C* AXIS IR SPECTRA OF Bi2201, Bi2212, AND Bi2223 SINGLE CRYSTALS

Figure 3 shows the real parts of the *c* axis optical conductivity $\sigma_1(\omega)$ and the dielectric function $\epsilon_1(\omega)$ at 150 K for the Bi2212 and Bi2223 single crystals with $T_c = 91$ K and $T_c = 107$ K. It is evident that the optical spectra look rather similar for both compounds. This is a consequence of the generic structural features of these two compounds. The electronic background is extremely weak and the spectra are dominated by the contributions of several IR-active phonon modes. Using the classical dispersion analysis we fit a set of Lorentzian oscillators simultaneously to $\epsilon_1(\omega)$ and $\epsilon_2(\omega)$ in the investigated spectral range. To describe the weak and rather flat electronic background in a Kramers-Kronig consistent way we have also included a sum of a Drude term and several very broad Lorentzian oscillators. As for the present purpose this description is rather formal we only limited the half-widths of the

TABLE VI: Frequencies ν_j (in cm^{-1}), oscillator strengths S$_j$, and damping parameters γ_j (in cm^{-1}) of the TO phonon bands observed in the c-polarized $\epsilon_2(\omega)$ spectra (T = 150 K) of the single crystals Bi2201, Bi2212, and Bi2223. The assignment with the calculated frequencies of A$_{2u}$ ($I4/mmm$) eigenmodes is given.

Bi2212			Bi2223			Bi2201		
$\nu_j(S_j)$	γ_j	A$_{2u}$	$\nu_j(S_j)$	γ_j	A$_{2u}$	$\nu_j(S_j)$	γ_j	A$_{2u}$
97	–	93	97	–	88	109 (0.56)	5.00	77
–	–	–	127 (0.10)	9.1	145	–	–	–
168 (0.29)	8.7	195	170 (0.63)	11.2	211	165 (0.45)	12.3	175
210 (0.34)	12.7	304	212 (0.77)	21.4	252	208 (0.65)	14.5	–
282 (0.16)	12.3	–	277 (0.50)	17.4	–	–	–	–
304 (1.13)	21.7	343	305 (1.43)	27.6	335	301 (1.31)	24.7	293
358 (0.33)	30.7	403	360 (0.46)	30.7	378	385 (0.85)	25.2	353
–	–	–	402 (0.16)	24.0	516	–	–	–
462 (0.02)	10.5	–	466 (0.02)	10.5	–	–	–	–
521 (0.22)	85.3	–	512 (0.26)	81.0	–	501 (0.10)	48.0	–
583 (0.65)	38.2	643	582 (0.61)	41.9	666	586 (0.42)	31.2	596
640 (0.03)	17.8	–	640 (0.03)	17.8	–	639 (0.01)	12.5	–
$\epsilon_\infty = 4.91$			$\epsilon_\infty = 5.77$			$\epsilon_\infty = 4.69$		

broad Lorenzians to values between 150 and 500 cm^{-1}. In Table 6 we list the frequencies ν_j, oscillator strengths S_j, and damping parameters γ_j of the TO phonon bands observed in the $\epsilon_2(\omega)$ spectra of Bi2212 and Bi2223 single crystals, together with determined values of the high-frequency dielectric constants, ϵ_∞.

For the Bi2223 we assign the main phonon bands at 97, 127, 170, 212, 305, 360, 402, and 582 cm^{-1} to the eight A$_{2u}$ character modes. These modes are clearly identified especially due to the resonance features in $\epsilon_1(\omega)$ as shown in Figure 3(b). Except for the two new intrinsic phonon modes in Bi2223 which appear at 127 and 402 cm^{-1}, the modes are observed at similar frequencies in both compounds. We believe that the remaining phonon features in Figure 3 around 277, 466, and 640 cm^{-1} are beyond the tetragonal $I4/mmm$ approximation,

as discussed in Section 2. The feature at 640 cm^{-1} appears to be a weak satellite of the pronounced high-frequency mode at 583 cm^{-1}. It is likely related to the effects of characteristic incommensurate modulations which induce strong distortions in the SrO and BiO planes. Indeed, this feature almost disappears with Pb doping which significantly reduces these superstructural modulations [13, 38]. Concerning the mode at 277 cm^{-1}, on the low-frequency side of the pronounced band at 305 cm^{-1}, we find that its oscillator strength correlates with the amount of extra-stoichiometric oxygen that is incorporated within the $Bi_2O_{2+\delta}$ bilayer during the oxygen annealing treatment [7]. By contrast to the 640 cm^{-1} satellite this feature remains persistent with Pb doping [38]. As a very weak feature at around 466 cm^{-1} is quite distant from the main phonon features we associate with the A_{2u} character modes, we would suggest that it is due to a contribution from some in-plane oxygen-related (O2 or O3) B_{2u} mode which has a $z(c)$ component (see Tables 3 and 5), or it can be a "disorder-induced" defect mode.

The 150 K spectra of the real parts of the c axis optical conductivity $\sigma_1(\omega)$ and dielectric function $\epsilon_1(\omega)$ of the as-grown nonsuperconducting Bi2201 single crystal, with the stoichiometric composition $Bi_2Sr_2CuO_6$, are shown in Figure 4. The values of the fitted frequencies ν_j, oscillator strengths S_j, and damping parameters γ_j of the TO phonon bands in the $\epsilon_2(\omega)$ are also listed in Table 6. To the best of our knowledge this is the first report of the c-polarized phonon spectra of the Bi2201 single crystal. Also we would like to note that the c axis spectra of the Bi2201 reported here exhibit remarkable difference with respect to those of the isostructural single layer Tl compound Tl2201 [13]. Six strong TO phonon features at around 109, 165, 208, 301, 385, and 586 cm^{-1} are clearly identified in the $\sigma_1(\omega)$ spectrum of Bi2201, as shown in Figure 4(a), whereas only five A_{2u} character modes are expected from the consideration in the ideal $I4/mmm$ space group (see Tables 1 and 2). In addition to a weak satellite feature at around 640 cm^{-1}, which we have already discussed in the previous paragraph, one "extra" mode appears at low frequencies in the Bi2201. This presumably reflects that the deviation from the tetragonality is most pronounced for the single layer Bi2201. We expect significant amplitudes in the c-polarized IR spectrum for the tetragonal forbidden B_{1u} mode of the Bi atoms, which are known to deviate most strongly from the tetragonal symmetry. We can also suggest that one new B_{1u} mode associated with the (2e) site position of the Cu1 atoms in the *Amaa* Bi2201, which is tetragonal silent, can appear in the orthorhombic symmetry (see Table 3). Also we have found that the spectra of

superconducting Bi2201 crystals with T_c varying between 3.5 and 8.5 K depending on the Bi/Sr ratio and the oxygen stoichiometry exhibit almost the same phonon features.

We have furthermore investigated the oxygen isotope effect for ^{16}O and ^{18}O substitution in Bi2212 as shown in Figure 5. For a mode with predominantly oxygen character the expected red shift of the eigenfrequency should be proportional to $[m(^{16}O)/m(^{18}O)]^{1/2}$ - 1, i. e. about 5.7%. A lower value of this so-called isotopic frequency shift signals that the corresponding phonon mode contains a significant contribution from the heavier (metal) ions. As shown in Figure 5(a), a noticeable red shift upon ^{18}O substitution is observed for the four A_{2u} phonons at 210, 304, 358, and 583 cm^{-1}; the estimated values of the shifts are 4.1, 4.4, 5.3, and 5.5%, respectively. This result confirms the expected trend that the three high frequency modes at 304, 358, and 583 cm^{-1} have predominantly oxygen character. It is an interesting finding that the low-frequency mode at 210 cm^{-1} also exhibits a sizeable red shift, which suggests that it contains a significant contribution from the oxygen vibrations.

Some of the *c*-polarized IR phonon modes in the bilayer Bi2212 and trilayer Bi2223 compounds exhibit strongly anomalous temperature dependence at T_c, accompanied with the development of a sizable absorption peak below T_c in the FIR range [2, 5, 6, 7] . Figures 6(a,b) show the real part $\sigma_1(\omega)$ of the c axis optical conductivity of the Bi2212 and Bi2223 compounds at two different temperatures, above T_c and well below T_c. In the normal state the spectra exhibit hardly any noticeable changes, except for a sharpening of the phonons with decreasing temperature. Right below T_c, however, the spectra change appreciably. This is also illustrated in Figure 6(c) which displays the difference $\sigma_1(T << T_c, \omega) - \sigma_1(T \gtrsim T_c, \omega)$. The most prominent feature is the broad absorption band around 500-550 cm^{-1} which appears below T_c and grows rapidly with decreasing temperature. This absorption band has been identified in both Bi2212 and Bi2223 and has been attributed to the transverse Josephson-plasma resonance (t-JPR) that is a universal feature of the multilayer high-T_c cuprate compounds [2, 4, 6]. It is evident from Figure 6 that the formation of the t-JPR is associated with an anomalous temperature dependence of the phonon modes at 360, 402 (specific for trilayer Bi2223) and 582 cm^{-1} denoted by A, B and C in Figure 6. The principal difference between the phonon anomalies observed in the bilayer and trilayer Bi-systems at T_c is that in the latter system the changes of the spectral weight of the apical phonon mode are much more pronounced and the additional phonon mode exhibiting the opposite temperature dependence is observed at 402 cm^{-1}.

V. THEORETICAL CALCULATIONS

A. Shell model approximation and potential parameters

To estimate the frequencies at which the various eigenmodes appear and, consequently, to make the assignment in the experimental phonon spectra (at T = 150 K), we have performed lattice-dynamical calculations using the shell model approximation. We performed the calculations for the three Bi-based structures Bi2201, Bi2212, and Bi2223 within the ideal tetragonal $I4/mmm$ (D_{4h}^{17}) space group, using the lattice constants and internal z structural parameters reported in Refs. [27, 28]. Screening has not been taken into account in this modeling. But screening should not noticeably affect the IR phonons along the poorly conducting c axis direction which we investigate in this work. Moreover, according to the study of the phonon screening of the in-plane IR-active modes in high-T_c superconductors the majority of the lattice modes have oscillator strength similar to those found in the undoped insulating materials [39]. This surprising result is explained by the inhomogeneous charge distribution in the CuO_2 planes due to which the ionic cores are no longer effectively screened, and the carriers will not be able to effectively screen the induced dipole moment [39]. Therefore, we apply the shell model approach suggesting that that screening due to free charge carriers should not have major effects [23]. Earlier the shell model approach has been successfully applied to study lattice dynamics and various physical properties of high-T_c superconductors [14, 17, 24, 25]. Our calculations are performed using the GULP code [26]. In the context of the shell model, the lattice is considered as an assembly of polarizable ions, represented by massive point cores and massless shells coupled by isotropic harmonic forces. The interaction includes contributions from Coulomb and short-range interactions. Short-range interactions between relatively small cations are usually ignored. The core and shell charges and the spring constant of each ion are parameters of the model. The short-range potentials used for the shell-shell interactions are of the Buckingham form

$$V_{ij} = A_{ij} exp(-r/\rho_{ij}) - C_{ij}/r^6. \quad (1)$$

The Buckingham potential parameters as well as the atoms' core and shell charges and the relevant spring constants were fitted in this work. To obtain a self-consistent set of the shell model parameters acceptable for a family of Bi-based high-T_c cuprates, we performed fits simultaneously to the structures of Bi2201, Bi2212, and Bi2223. As the starting values for

the shell model parameters – pair potentials, net ionic charges, shell and core charges and relevant spring constants – we used the ones obtained by Baetzold [24] for a bilayer cuprate $YBa_2Cu_3O_{7-\delta}$ system. We have two reasons to keep the net ionic charges of the atoms in the cuprate planes of +2| e | for Cu1 and Cu2, and -2| e | for O1 and O4 . First, it is in line with the approach of Baetzold for Y123 [24] and second, this is required if we want to describe single, bi- and trilayer Bi-systems by the same set of the potential parameters. Otherwise, by dividing the non-integer charges between the cuprate planes we would have different pair potential parameters in each case. Following the approach of Baetzold, we also keep the same effective charges of -1.67| e | for O2 and O3. We take the formal ionic charge +2| e | for Sr, and to satisfy the electroneutrality conditions we have to assume an effective charge +2.33| e | for Bi. The formal charges here describe the dipole moment per unit displacement, rather than the charge within some region of space. It was noted by Catlow and Stoneham that even the integer charge-distribution method can be successfully employed to accurately calculate physical properties of solids where ionicity may vary over a range of values [40]. We assume the shell charge of -3.2576| e | for all oxygen ions, as in [24]. The Sr, Bi, Ca and O ions are treated as polarizable, while the Cu ions are treated as unpolarizable. The fitting procedure keeps O-O (shell-shell) interaction as those of typical oxides [41, 42]. The structures were allowed to relax to equilibrium conditions under the symmetry ($I4/mmm$) restrictions, the cores and shells were allowed to move separately. The forces on the atoms were minimized by varying the potential parameters, the eigenvalues for the first three modes for all three compounds had approximately zero values, indicating a stable structure in each case. Normally a good fit requires some information on physical properties - elastic, dielectric, and piezoelectric (where applicable) constants - as well as the structure. In general, vibrational frequencies contain far more information than any of the above. However, in fitting the frequencies a reasonable implication for the assignment has to be suggested, at least for some key modes. In the present work a final fit was done to the available experimental data on the bilayer Bi2212 compound. The criterion of a successful fit was good agreement with the structural parameters [27], provided that approximately zero forces are applied for all atoms, with the c axis static ϵ_0 and high-frequency ϵ_∞ dielectric constants, and with the frequencies of the c axis IR- and Raman-active optical phonons [43]. The resulting Buckingham potential parameters, ionic shell charges (Y) and force constants (k) are presented in Table 7. To simulate different in-plane and out-of-plane bond lengths

TABLE VII: Potential parameters for short-range shell-shell interactions (Eq. (1)), ion shell charges (Y) and force constants (k) in tetragonal $I4/mmm$ (D_{4h}^{17}) $Bi_2Sr_2CuO_6$, $Bi_2Sr_2CaCu_2O_8$, and $Bi_2Sr_2Ca_2Cu_3O_{10}$; in-plane O1 and O4 oxygen ions are taken of a net charge – 2.0 | e |, out-of-plane O2 and O3 oxygen ions are taken of a net charge – 1.67 | e |, r_{cutoff} = 99Å.

	A(eV)	ρ(Å)	C(eV·Å^{-6})
Cu1-O1; Cu2-O4	3889.8	0.24273	0.00
Cu1-O2,O4; Cu2-O1	2708.0	0.22074	0.00
Ca-O1; Ca-O4	14882.2	0.24203	0.00
Sr-O1	1487.9	0.33583	0.00
Sr-O2	20097.2	0.24823	0.00
Sr-O3	30202.0	0.24823	0.00
Bi-O2	15671.0	0.22074	0.00
Bi-O3	147997.9	0.22074	0.00
Cu1-Sr	167925.4	0.22873	0.00
Sr-Sr	3680.5	0.25880	0.00
Sr-Bi	158000.0	0.22873	0.00
Bi-Bi	7100.0	0.22873	0.00
Ca-Ca	4500.0	0.22873	0.00
O-O	22764.0	0.14900	75.00

Ion	Y (| e |)	k (eV ·Å^{-2})
Ca	2.00	99.0
Cu1, Cu2	2.00	999999.0
Bi	2.33334	27.2
Sr	5.09995	146.7
O1	-3.25760	26.0
O4	-3.25760	76.0
O2, O3	-3.25760	100.0

TABLE VIII: A comparison between the experimental and calculated structures of Bi2212, Bi2223, and Bi2201 ($I4/mmm$ (D_{4h}^{17})). Experimental values of the fractional atomic coordinates and corresponding calculated values are given, with the experimental errors for Bi2212 structure shown in brackets.

	Bi2212		Bi2223		Bi2201	
	z, exp.	z, calc.	z, exp.	z,calc.	z, exp.	z, calc.
Ca	0.00	0.00	0.0443	0.0464	–	–
Sr	0.1097(5)	0.1096	0.1346	0.1369	0.0759	0.0696
Bi	0.3022(3)	0.3043	0.292	0.297	0.3148	0.3175
Cu1	0.4456(9)	0.4334	0.4109	0.4010	0.00	0.00
Cu2	–	–	0.00	0.00	–	–
O1	0.446(3)	0.445	0.411	0.408	0.00	0.00
O2	0.375(4)	0.372	0.353	0.352	0.405	0.401
O3	0.205(4)	0.211	0.213	0.219	0.194	0.201
O4	–	–	0.00	0.00	–	–

in the structures of Bi-based compounds, as well as anisotropy of oxygen polarizability, generally we have arrived at different pair potentials for the Cu-O, Sr-O, and Bi-O in-plane and out-of-plane short-range interactions. It is particularly remarkable that the pair potentials for the Bi-O2 and Bi-O3 short-range interactions are significantly different, and this fact seems to be mainly due to very different Bi-O bond lengths, i.e., in the structures of Bi-based compounds we have the Bi-O2 bond length of 2.22 $\mathring{A}$, the in-plane Bi-O3 bond length of 2.71 $\mathring{A}$, and the longest Bi-O3 bond length, between weakly coupled Bi_2O_2 biplanes, of 2.97 $\mathring{A}$ [27]. Thus elaborated, our shell model parameters allow us to describe all three Bi-based structures by the same set of short-range pair-potential parameters, listed in Table 7. To compare the experimental and calculated structures we present experimental values of the fractional atomic coordinates obtained from Refs. [27, 28] and the corresponding calculated values in Table 8, where we also show the experimental errors for the Bi2212 fractional coordinates [27] in brackets. As far as our final fit is based on the Bi2212 crystal, the best agreement with the internal structural parameters is naturally obtained for this system. As can be seen from Table 8 these parameters reproduce also reasonably well the

Bi2223 and Bi2201 structures. Slightly varying the shell model parameters we can arrive at a better agreement with the particular structure chosen, although we would rather aim to obtain a self-consistent set of shell model parameters, which can account for the common generic features in all three Bi-based structures. Going ahead, we would like to mention here that this would not qualitatively affect the character of the eigenmodes resulting from our shell model calculations, although the eigenfrequencies and amplitudes of the eigenvectors of the c axis phonon modes can slightly change. The elastic properties calculated with these parameters do not exhibit unphysical (i.e., negative values), and the eigenvalues for the first three modes have approximately zero values in all three compounds which is indicative of a stable structure. We have also arrived at a good agreement with the experimental values for dielectric constants. All three compounds Bi2212, Bi2223, and Bi2201 have close values of c axis dielectric constants within the range $\epsilon_0 \simeq 9.5 \div 12.0$ and $\epsilon_\infty \simeq 4.9 \div 5.8$, as estimated from our experimental $\epsilon_1(\omega)$ and $\epsilon_2(\omega)$ spectra. The corresponding calculated values fall in the range $\epsilon_0 \simeq 10.9 \div 13.9$ and $\epsilon_\infty \simeq 4.8 \div 5.6$. Certainly, the obtained set of shell mode parameters is not unique. Nevertheless, given the fact that by using the same set of parameters we can reproduce the structures and main phonon bands as observed for all three compounds we obtain more confidence in the assignment for the phonon modes.

B. Calculated Γ-point A_{2u} symmetry modes in Bi2201, Bi2212 and Bi2223

In Figure 7 we show the eigenvector patterns corresponding to six eigenmodes of A_{2u} symmetry and one silent mode of B_{2u} symmetry for the Bi2212, resulting from our lattice-dynamical calculations. Under each patch we list values of the eigenfrequencies and below we make an assignment based on a comparison with the experimental frequencies of the TO phonon bands observed in the c-polarized spectra of the Bi2212 single crystal (T = 150 K, see Figure 3 and Table 6). Mixing due to out-of-phase motion of ions of equal symmetry in inequivalent positions often does not allow the determination of a unique character for a given set of equal symmetry modes. The total number of the modes in each symmetry, of course, is unaffected by mixing. The character of the assigned modes is determined according to the dominant contribution from the atoms participating in the vibration and shown atop. The respective calculated components of the eigenvector amplitudes are given in Table 9. The lowest frequency mode calculated at 93 cm^{-1} (experimentally observed at 97 cm^{-1}, see

Figure 3 and Ref. [5]) is related to motion of the heavy Bi atoms, which is strongly mixed with out-of-phase motion of Sr, Cu1 and Ca, with a small oxygen contribution from different crystallographic planes. The next mode of A_{2u} symmetry calculated at 195 cm^{-1} (168 cm^{-1}) is predominantly due to motion of the Cu1 against Sr, with a small contribution from the Ca ions. The A_{2u} mode at 304 cm^{-1} (210 cm^{-1}) is due to the vibrations of Ca and O1 ions against Sr and O3. This mixed low-frequency mode contains noticeable contribution from the copper-plane O1 ions and bismuth-plane O3 ions to the c axis oscillations. The three high-energy vibrations are predominantly oxygen-related. The mode calculated at 343 cm^{-1} (304 cm^{-1}) is basically due to O3 and O1 vibrations against Sr and Ca atoms, with a predominant contribution from the bismuth-plane oxygen O3. The Cu-O bond-bending character mode at 403 cm^{-1} (358 cm^{-1}) involves significant contribution from the copper-plane O1 ions, vibrating against the Ca and O3 atoms. The highest frequency mode at 643 cm^{-1} (583 cm^{-1}) is due to O2 and O3 out-of-phase oscillations, and it has apparently apical character due to predominant contribution from the strontium-plane O2 oscillations along the c axis. Our assignment for the c-polarized phonon modes is confirmed by the oxygen isotope effect in the Bi2212 single crystal, investigated in this work (see Figure 5). A noticeable red shift upon ^{18}O substitution is observed for the four c axis phonons at 210, 304, 358, and 583 cm^{-1}; the estimated values of the shifts are 4.1, 4.4, 5.3, and 5.5%, respectively. This result is consistent with our assignment that suggests that the three high-frequency modes have predominantly oxygen character. In addition, according to our assignment, the low-frequency mode at 210 cm^{-1} also contains appreciable contribution from the copper-plane O1 and bismuth-plane O3 atoms, thus consistent with the noticeable red shift with the ^{16}O for ^{18}O substitution. The present theoretical shell model calculations thus reproduce the frequencies of the c axis A_{2u} eigenmodes quite well for the bilayer Bi2212 single crystal. We would like to notice that although the eigenfrequencies are somewhat different the character of A_{2u} vibrations resulting from the present shell model calculations for the Bi2212 system is quite consistent with the earlier calculations, made by Prade *et al.* [14].

In Figure 8 we show the eigenvector patterns corresponding to the eight eigenmodes of A_{2u} symmetry and two silent modes of B_{2u} symmetry for the Bi2223, resulting from our lattice-dynamical calculations with the same set of the shell model parameters listed in Table 7. The calculated components of the eigenvector amplitudes are summarized in Table 9. We

make an assignment of the TO phonon modes observed in the c axis ellipsometry spectra of the Bi2223 single crystal (T = 150 K, see Figure 3 and Table 6) based on a comparison with the present calculations. As can be seen from Figures 7 and 8, close similarity with the Bi2212 is observed for their eigenmode characters and eigenfrequency values due to the common generic features in the Bi2212 and Bi2223 structures. The only exception is that two new additional modes of A_{2u} symmetry are present for the trilayer Bi2223 system. Our calculations give one additional mode for Bi2223 at 145 cm^{-1}, its character is defined by the main contribution from the Cu2 (from the inner CuO_2 plane) and Sr out-of-phase vibrations, and assigned it with the new mode clearly discernible in the $\epsilon_1(\omega)$ spectrum at 127 cm^{-1} (see Figure 3(b)), which is also in agreement with the results of IR measurements done very recently on an oriented ceramics of Bi2223 [19]. We calculated four A_{2u} "light", predominantly oxygen-related, modes at the following frequencies 335, 378, 516, and 666 cm^{-1}. Like in the Bi2212, the highest-frequency mode at 666 cm^{-1} (581 cm^{-1}) is associated with the out-of-phase O2 and O3 vibrations, the mode calculated at 335 cm^{-1} (304 cm^{-1}) is predominantly due to the Bi-plane O3 oscillations, and the mode calculated at 378 cm^{-1} (359 cm^{-1}) is the Cu-O bond-bending character mode, corresponding to the out-of-phase motion of the Ca atoms and oxygens O1 in the outer CuO_2 planes. We calculated one additional oxygen-related mode in the Bi2223 at 516 cm^{-1}, and its character is defined by the out-of-phase vibrations of the Ca atoms and oxygens O4 in the inner CuO_2 plane. We assign it with the new mode appearing in c axis the phonon spectrum of the Bi2223 at 402 cm^{-1}, as it is clearly observable in Figure 3, and also in agreement with the results of [19].

As we discussed in Section 4 some of the c-polarized IR phonon modes in the bilayer Bi2212 and trilayer Bi2223 compounds exhibit a strongly anomalous temperature dependence at T_c, accompanied with the development of a sizable absorption peak below T_c in the FIR range, as illustrated in Figure 6 [2, 5, 6, 7]. The two most pronounced phonon bands at 304 and 582 cm^{-1} appear at the same frequencies in the c axis ellipsometry spectra of the Bi2212 and Bi2223. According to our assignment they are associated with the predominant contribution from the BiO layer O3 oxygens and the apical O2 oxygens, respectively. It is evident from Figure 6 that the formation of the t-JPR in Bi2212 and Bi2223 is accompanied with the strongly anomalous temperature dependence of the phonon modes at 360, 402 (specific for trilayer Bi2223) and 582 cm^{-1} denoted by A, B, C. An explanation of the anomalous changes of the phonon modes at 360 and 402 cm^{-1} upon entering the superconducting state

has been recently proposed based on the so-called Josephson superlattice model, assuming that these bands belong to the vibration of the planar oxygens [6, 7]. This assumption is supported by our assignment which suggests that these modes are bond-bending character modes which involve a significant contribution from the outer copper-plane O1 and inner copper-plane O4 ions, respectively.

In Figure 9 we present the eigenvector pattern corresponding to the five eigenmodes of A_{2u} symmetry for Bi2201, the calculated components of the eigenvector amplitudes are listed in Table 9. We have calculated two A_{2u} symmetry modes at low frequencies. The calculated lowest frequency mode is related to the motion of the heavy Bi atoms, which is strongly mixed with out-of-phase motion of Sr and Cu1. The next mode of A_{2u} symmetry is predominantly due to the motion of Cu1 against Sr. The three phonon features are clearly observed in the c axis ellipsometry spectra of the Bi2201 at low frequencies at around 109, 165, and 209 cm^{-1} (see Figure 4 and Table 6); in Section 4 we have already discussed the possible reasons for the appearance of one "extra" phonon feature. We have made an assignment of the modes at low frequencies by analogy with the vibration characters at the corresponding frequencies in the B2212 and Bi2223 crystals. The three high-energy vibrations are predominantly oxygen-related. The highest frequency mode at 596 cm^{-1} (586 cm^{-1}) has apparently apical character due to the predominant contribution from the strontium-plane O2 oscillations along the c axis. The modes calculated at 293 cm^{-1} and 353 cm^{-1} are basically due to bismuth-plane O3 and copper-plane O1 mixed in-phase and out-of-phase vibrations, respectively, and they correlate well with the experimental frequencies at 301 and 385 cm^{-1}. In the Bi2201 the CuO_2 planar oxygen band located at 385 cm^{-1} has much larger intensity than in the Bi2212. This is very probable due to the fact that in the Bi2212 the CuO_2 planar oxygen mode is, already in the normal state, strongly renormalized by its coupling to interlayer electronic excitations.

C. Calculated Γ-point A_{1g} symmetry modes in Bi2201, Bi2212 and Bi2223

In this Section we just briefly discuss the results of our shell model calculations for the Raman-active modes in the three Bi-based compounds and suggest the assignment for the phonon modes observed in the experimental spectra. It has been generally found that a larger number of phonon modes occur in the Raman spectra of the Bi-based compounds than would

TABLE IX: Calculated components of eigenvectors of A_{2u} modes in Bi2201 ($Bi_2Sr_2CuO_6$), Bi2212 ($Bi_2Sr_2CaCu_2O_8$) and Bi2223 ($Bi_2Sr_2Ca_2Cu_3O_{10}$) crystals in tetragonal $I4/mmm$ (D_{4h}^{17}) space group.

Bi2212	Bi(z)	Sr(z)	Cu1(z)	–	Ca(z)	O1(z)	O2(z)	O3(z)	–
93 cm^{-1}	-0.46	0.27	0.33	–	0.29	0.16	-0.07	-0.11	–
195 cm^{-1}	-0.04	0.43	-0.54	–	0.16	0.05	-0.01	0.00	–
304 cm^{-1}	-0.09	0.33	0.10	–	-0.76	-0.15	0.08	0.18	–
343 cm^{-1}	-0.11	-0.18	-0.09	–	-0.15	0.31	0.13	0.46	–
403 cm^{-1}	0.09	-0.01	-0.04	–	-0.50	0.29	-0.15	-0.41	–
643 cm^{-1}	0.07	0.04	0.03	–	0.01	-0.01	-0.66	0.24	–
Bi2223	Bi(z)	Sr(z)	Cu1(z)	Cu2(z)	Ca(z)	O1(z)	O2(z)	O3(z)	O4(z)
88 cm^{-1}	-0.45	0.11	0.14	0.57	0.21	0.08	-0.07	-0.11	0.17
145 cm^{-1}	-0.23	0.33	0.22	-0.68	0.09	0.10	0.00	-0.01	-0.09
211 cm^{-1}	0.01	0.27	-0.59	-0.06	0.23	0.06	-0.03	0.00	0.09
252 cm^{-1}	-0.05	0.42	-0.05	0.29	-0.49	-0.07	0.02	0.03	-0.16
335 cm^{-1}	-0.09	-0.15	-0.07	-0.01	-0.21	0.29	0.10	0.46	0.16
378 cm^{-1}	0.10	-0.09	-0.05	0.09	-0.13	0.34	-0.14	-0.41	0.04
516 cm^{-1}	0.05	0.05	0.03	-0.21	-0.23	-0.05	-0.08	-0.22	0.60
666 cm^{-1}	0.08	0.03	0.05	0.00	0.01	-0.01	-0.66	0.22	0.02
Bi2201	Bi(z)	Sr(z)	Cu1(z)	–	–	O1(z)	O2(z)	O3(z)	–
77 cm^{-1}	-0.31	0.24	0.77	–	–	0.10	-0.11	-0.17	–
175 cm^{-1}	-0.21	0.51	-0.56	–	–	0.17	0.02	-0.06	–
293 cm^{-1}	-0.24	-0.09	0.08	–	–	0.30	0.15	0.56	–
353 cm^{-1}	0.10	-0.23	-0.08	–	–	0.59	-0.10	-0.27	–
596 cm^{-1}	0.09	0.06	-0.05	–	–	0.00	-0.66	0.23	–

be expected from the simple tetragonal $I4/mmm$ symmetry consideration (given in Tables 1 and 2). As a result different groups have reported rather different and then contradictory assignments. We have already referred to these reasons in Section 2. There appears to be a consensus on the origin of the strong B_{1g} phonon in Raman spectra of Bi2212. From

the B_{1g}-symmetry selection rules the peak at about 285 cm^{-1}, which occurs only in the $z(xy)\bar{z}$ spectrum can be assigned to the O(1) B_{1g} phonon characterized by out-of-phase motion of the oxygen atoms in the CuO_2 plane. This is not the case, however, for two of the strongest A_{1g} modes that appear in the Raman spectrum at higher frequencies around 460 and 620 cm^{-1}. The origin of the high-frequency vibrations in the Raman spectrum of Bi2212 remains controversial despite many investigations by different groups. Most authors have assigned the 460 cm^{-1} mode to the vibrations of the apical oxygen atoms located in the SrO planes and the 620 cm^{-1} phonon to vibrations of the oxygen atoms located in the BiO planes [9, 45, 47]. However, recently it was argued that the assignment should be reversed [48, 49]. It was shown that these two bands exhibit different polarization dependencies for the incident and scattered vectors, indicating that the degree of mode mixing is small, and the 620 cm^{-1} band is strongly c -polarized like apex oxygen vibrations characteristic for most high-T_c superconductors [48]. Moreover, the 460 cm^{-1} band has been found to soften at a significantly faster rate than the 620 cm^{-1} band with ^{18}O oxygen isotope substitution, in agreement with the more liable oxygen atoms from the BiO layer [49]. Therefore, in fitting our shell model parameters for the Bi2212 crystal we have implied an assignment for the mode observed at around 285 cm^{-1} as the B_{1g} mode, whereas for the modes observed at around 460 and 620 cm^{-1} as the A_{1g} modes associated with the O3 (from the BiO plane) and O2 (from the SrO plane) predominant contributions, respectively.

In Figure 10 we show our suggested eigenvector pattern corresponding to the six eigenmodes of A_{1g} symmetry and one B_{1g} symmetry for the Bi2212 crystal. We list values of the eigenfrequencies and below we make an assignment in agreement with the experimental Raman study of $Bi_2Sr_2Ca_{1-x}Y_xCu_2O_{8+\delta}$ ($x = 0 \div 1$) single crystals [48]. A number of phonons observable below 400 cm^{-1} in the Raman spectra in the A_{1g} (or A_g) scattering configurations are considered by Kakihana *et al.* as "disorder-induced" modes [48]. In addition, as a weak satellite feature at $\sim$ 657 cm^{-1} near the strong phonon band at 620 cm^{-1} disappears in modulation-free $Bi_{2-x}Pb_xSr_2Ca_{1-x}Cu_2O_{8+\delta}$ crystals it is possibly induced by the incommensurate superstructural modulation [50]. Another satellite feature at $\sim$ 458 cm^{-1} near the pronounced phonon band at 460 cm^{-1} is possibly associated with extra oxygen atoms in the BiO layers, and also referred to "disorder-induced" scattering.

In Figure 11 we show the eigenvector pattern corresponding to the seven eigenmodes of A_{1g} symmetry and one B_{1g} symmetry for the Bi2223 crystal, calculated using the same

basic set of the shell model parameters. From Figures 10 and 11 we can see that due to the common generic features in the Bi2212 and Bi2223 structures the vibration characters are similar and the eigenfrequency values are close for the corresponding eigenmodes. This is consistent with the recently published results on Raman measurements showing that frequencies of the major phonon bands are almost identical in Bi2212 and Bi2223 single crystals [52]. The exception is an additional mode of the A_{1g} symmetry present in the trilayer Bi2223 crystal. Comparing the bilayer and trilayer systems (Figures 10 and 11) we can conclude that instead of one A_{1g} mode associated with the O1 vibrations in the CuO_2 plane in the Bi2212 structure, calculated at 370 cm^{-1}, in the Bi2223 structure we have two A_{1g} modes associated with the Ca and O1 (from the outer CuO_2 planes) in-phase and out-of-phase vibrations, calculated at 316 and 391 cm^{-1}, respectively.

In Figure 12 we show the eigenvector pattern corresponding to the four eigenmodes of A_{1g} symmetry for the $I4/mmm$ Bi2201, resulting from our shell model calculations. As usual many more phonon modes are observed in the experimental Raman spectra implying that the simple tetragonal approximation is no more applicable for the interpretation of the Raman phonon spectra of the Bi2201. In Tables 1 and 3 we show that due to the orthorhombic distortions the O1 atoms in the CuO_2 plane become "Raman-active", and, as a result, a number of new Raman-active modes of A_g, B_{1g}, $2B_{2g}$, and $2B_{3g}$ character will appear in the *Amaa* Bi2201. We suggest that a more appropriate approximation for the interpretation of the Γ-point Raman-active phonons in this compound will be the orthorhombic *Amaa* space group. However, the assignment for the two high-frequency oxygen modes (as we show in Figure 12) is the same as for the Bi2212 and Bi2223 crystals, and the calculated frequencies agree quite well for these three compounds.

Resonant Raman scattering below T_c has been discovered in Bi- and Hg-based high T_c compounds with three or four CuO_2 layers [51, 52, 53]. Strong superconductivity-induced enhancement of the phonons at 260 and 390 cm^{-1}, together with the development of a broad band peaking at around 580 cm^{-1}, has been observed in the recent resonant Raman scattering study on the Bi2223 single crystal with T_c = 109 K [52]. Our measurements of resonant Raman scattering (E_{exc} = 2.18 eV) done on our Bi2223 single crystal with lower T_c = 107 K reproduce the results of Limonov *et al.* In Figure 13(a) we show the Raman spectra at two different temperatures, i.e. somewhat above and well below T_c. Figure 13(b) shows the difference between these Raman spectra. Our data clearly demonstrate

the superconductivity-induced enhancement of the phonon bands at 260 and 390 cm^{-1} and a broad band peaking around 550 cm^{-1}. There are two alternative explanations of these superconductivity-induced anomalies in multilayer high-T_c compounds; one considers the broad excitation band as a "pair-breaking" peak at 2Δ [52], and the another refer it to a Raman-active c axis plasmon [53]. A more detailed study of the doping effect on the resonance peak position is required to clarify its origin. Nevertheless, dicussing the phonon anomalies observed in trilayer Bi2223 we would like to notice that both approaches consider the superconductivity-induced anomalies as due to strong coupling of the intratrilayer electronic excitation with phonons which involve calcium and planar oxygen ions. Experimental resonant Raman scattering studies bring evidence in favour of our assignment suggested for the trilayer Bi2223 crystal (Figure 11). The superconductivity-enhanced phonon bands at 260 and 390 cm^{-1} in the Bi2223 can be ascribed to the A_{1g} in-phase and out-of-phase vibrations of the Ca atoms with oxygens in the outer CuO_2 planes, in agreement with our assignment for the A_{1g} modes calculated at 316 and 391 cm^{-1}.

VI. CONCLUSIONS

In summary, we present experimental data on single crystals as obtained by spectral ellipsometry and make the assignment of the IR c axis polarized phonon modes in single, bi-, and trilayer bismuth compounds (Bi2201, Bi2212, and Bi2223) by comparing them with the results of the shell model calculations. The c axis IR phonon spectra look very similar for the bilayer and trilayer Bi-based crystals, supporting experimental evidence for the generic structural features of these compounds. We apply a tetragonal $I4/mmm$ approximation in the interpretation of the c axis IR spectra of the Bi-based compounds, which are known to have pseudotetragonal structure, and conclude that this approximation provides a reasonable description of the main features in the phonon spectra. In the framework of this approximation, we have identified "disorder-induced" modes due to the orthorhombic distortions associated with the incommensurate superstructural modulations and extra-stoichiometric oxygen. Comparing with the bilayer Bi-system, we identify two additional c axis phonon modes in the ellipsometric spectra of the trilayer system, one at 127 cm^{-1}, among the "heavy" modes, and the another at 402 cm^{-1}, among the "light" modes, which according to our assignment involve significant contribution of the copper and oxygen atoms in the inner CuO_2

plane, respectively. The recent experimental observation of a Josephson-plasma-resonance and phonon anomalies in Bi2223 [7] provide, indeed, a strong support for the Josephson-superlattice model, which consistently explains, the phonon anomalies and the formation of a broad absorption band below T_c using the components of the eigenvector amplitudes for the relevant oxygen modes at 358 and 402 cm^{-1}. The two modes involving O3 (BiO plane) and O1 (CuO_2 plane) atoms exhibit substantial frequency changes in the single layer system, and appear at 294 and 389 cm^{-1}, respectively. For the single layer system the mode at 389 cm^{-1} increases dramatically in intensity. This evident difference between single and multilayer compounds in the behavior of this particular phonon mode reflects the fact that in multilayer compounds the oxygen bond-bending phonon mode is strongly-coupled with the electronic excitation due to the charge density oscillations between the closely spaced CuO_2 planes. In addition, we also show the eigenvector patterns and calculated frequencies for the Raman-active phonon modes of A_{1g} symmetry in these three compounds according to the results of the present shell model calculations. The supeconductivity-induced resonant Raman scattering for the two phonon modes at 260 and 390 cm^{-1} very recently observed in the trilayer Bi2223 single crystal [52] is well consistent with the suggested assignment.

VII. ACKNOWLEDGMENTS

The authors thank J. Gale for making available General Utility Lattice Program (GULP) used in the present calculations. We are grateful to R. Evarestov and E. Kotomin for fruitful discussions. T. Holden acknowledges support by AvH Foundation. We acknowledge L. Carr at NSLS and Y.-L. Mathis at ANKA for their support during the ellipsometry measurements.

---

[1] M. Grüninger, D. van der Marel, A. A. Tsvetkov, and A. Erb, Phys. Rev. Lett. **84**, 1575 (2000).

[2] D. Munzar, C. Bernhard, A. Golnik, J.Humlíček, M. Cardona, Solid State Commun. **112**, 365 (1999).

[3] D. van der Marel and A. A. Tsvetkov, Phys. Rev. B **64**, 024530 (2001).

[4] C. Bernhard, D. Munzar, A. Golnik, C. T. Lin, A. Wittlin, J. Humličcek, M. Cardona, Phys. Rev. B **61**, 618 (2000).

[5] V. Železný, S. Tajima, D. Munzar, T. Motohashi, J. Shimoyama, K.Kishio, Phys. Rev. B **63** 060502 (2001).

[6] D. Munzar, C. Bernhard, T.Holden, A. Golnik, J.Humlíček, M. Cardona, Phys. Rev. B **64** 024523 (2001).

[7] A. V. Boris, D. Munzar, N. N. Kovaleva,B. Liang, C. T. Lin, A. Dubroka, A. V. Pimenov, T. Holden, B. Keimer, Y.-L. Mattis, and C. Bernhard, Phys. Rev. Lett, **89** 277001-1 (2002).

[8] W. Kress and U. Shröder, Phys. Rev. B **38** 2906 (1988).

[9] R. Liu, C. Thomsen, W. Kress, M. Cardona, and B. Gegenheimer, F. W. Wette, J. Prade, and A. D. Kulkarni, U. Shröder, Phys. Rev. B **37** 7971 (1988).

[10] J. Humliček, A. P. Litvinchuk, W. Kress, B. Lederle, C. Thomsen, M. Cardona, H. -U. Habermeier, I. E. Trofimov, W. König, Physica C **206** 345 (1993).

[11] R. Henn, T. Strach, E. Schönher, and M. Cardona, Phys. Rev. B **55** 3285 (1997).

[12] S. Tajima, G. D. Gu, S. Miyamoto, A. Odagawa, and N. Koshizuka, Phys. Rev. B **48** 16164 (1993).

[13] A. A. Tsvetkov, D. Dulic, D. van der Marel, A. Damascelli, G. A. Kaljushnaia, J. I Gorina, N. N. Senturina, N. N. Kolesnikov, Z. F. Ren, J. H. Wang, A. A. Menovsky, T. T. M. Palstra, Phys. Rev. B **60** 13196 (1999).

[14] J. Prade, A. D. Kulkarni, F. W. de Wette, U. Schroder, W. Kress, Phys. Rev. B **39** 2771 (1989).

[15] Chun-Sheng Jia, Pi-Yuan Lin, Yang Xiao, Xiao-Wei Jiang, Xue-Yan Gou, Su Huo, Hao Li, Qiu-Bo Yang, Physica C **268** 41 (1996).

[16] Sheng Jia Chun and Shu Zhou Wu, Phys. Stat. Sol. B **163** K49 (1991).

[17] A. D. Kulkarni, F. W. de Wette, J. Prade, U. Schroder, W. Kress, Phys. Rev. B **41** 6409 (1990).

[18] T. Zetterer, M. Franz, J. Schützmann, W. Ose, H. H. Otto, and K. F. Renk, Phys. Rev. B **41** 9499 (1990).

[19] N. Petit, V. Garnier, V. Ta Phuoc, R. Caillard, A.-M. Frelin, A. Ruyter, I. Laffez, J.-C. Soret, A. Maignan, and F. Gervais, Eur. Phys. J. B **25** 423 (2002).

[20] B. Liang, C.T. Lin, P. Shang, G. Yang, Physica C **383** 75 (2002).

[21] B. Liang, C. T. Lin, J. Crystal Growth **237-239** 756 (2002); B. Liang, C. T. Lin, A. Maljuk, Y. Yan, Physica C **366** 254 (2002).

[22] B. Liang, A. Maljuk and C. T. Lin, Physica C **361** 156 (2001); C. T. Lin, B. Liang, M. Freiberg, K. Peters, E. Schoenherr, Physica C **341** 541 (2000).

[23] A. M. Stoneham and L. W. Smith, J. Phys.:Condens. Matter **3** 225 (1991).

[24] R. C. Baetzold, Phys. Rev. B **38** 11304 (1988).

[25] M. S. Islam, M. Leslie, S. M. Tomlinson, and C. R. A. Catlow, J. Phys. C **21** L109 (1988).

[26] J. D. Gale, Phil. Mag. B **73** 3 (1996); J. Chem. Soc. Faraday Trans. **93** 629 (1997).

[27] J. M. Tarascon, Y. Le Page, P. Barboux, B. G. Bagley, L. H. Greene, W. R. McKinnon, G. W. Hull, M. Giroud, D. M. Hwang, Phys. Rev. B **37** 9382 (1988).

[28] J. M. Tarascon, Y. Le Page, P. Barboux, B. G. Bagley, L. H. Greene, W. R. McKinnon, G. W. Hull, M. Giroud, D. M. Hwang, Phys. Rev. B **38** 8885 (1988).

[29] K. Imai, T. Kawashima, S. Sueno, A. Ono, Jpn. J. Appl. Phys. **27** L1661 (1988).

[30] C. C. Torardi, M. A. Subramanian, J. C. Calabrese, J. Gopalakrishnan, E. M. McCarron, K. J. Morrissey, T. R. Askew, R. B. Flippen, U. Chowdhry, A. W. Sleight, Phys. Rev. B **38** 224 (1988).

[31] A. Sequeira, H. Rajagopal, P. V. P. S. S. Sastry, J. V. Yakhmi and R. M. Iyer, Physica B, **174** 367 (1991).

[32] Y. Ito, A.-M. Vlaicu, T. Mukoyama, S. Sato, S. Yoshikado, C. Julien, I. Chong, Y. Ikeda, M. Takano, E. Ya. Sherman, Phys. Rev. B **58** 2851 (1998).

[33] P. Bordet, J. J. Capponi, C. Chaillout, J. Chenavas, A. W. Hewat, E. A. Hewat, J. L. Hodeau, M. Marezio, J. L. Tholence and D. Tranqui, Physica C **156** 189 (1988).

[34] E. Bellingeri, G. Grasso, R. E. Gladyshevskii, M. Dhalle, R. Flükiger, Physica C **329** 267 (2000).

[35] N. Jacubowicz, D. Grebille, M. Herview, H. Leligny, Phys. Rev. B **63** 214511 (2001) and references therein.

[36] D.J. Pringle, Phys. Rev. B **62**, 12527 (2000).

[37] R. Henn, C. Bernhard, A. Wittlin, M. Cardona, S. Uchida, Thin Solid Films **313-314** 643 (1998).

[38] A. V. Boris (unpublished).

[39] C. C. Homes, A. W. McConnell, B. P. Clayman, D. A. Bonn, Ruixing Liang, W. N. Hardy, M. Inoue, H. Negishi, P. Fournier, and R. L. Greene, Phys. Rev. Lett. **84** 5391 (2000).

[40] C. R. A. Catlow and A. M. Stoneham, J. Phys. C **16** 4321 (1983).

[41] C. R. A. Catlow, W. C. Mackrodt, M. J. Norgett, A. M. Stoneham, Philos. Mag. **35** 177 (1977).

[42] V. N. Popov, J. Phys.: Condens. Matter **7** 625 (1995).

[43] Our earlier fit of the shell model parameters was based on the experimental data only of the c-axis ir- phonons. Although these earlier calculations resulted, in principal, in the same assignment and character of the A_{2u} modes as the present calculations, we arrived at somewhat different eigenvalues of the A_{2u} modes, in particular for the Bi2223 presented in [7].

[44] V. Železný, S. Tajima, T. Motohashi, J. Shimoyama, K.Kishio, D. van der Marel, J. Low Temp. Phys. **117** 1019 (1999).

[45] M. Cardona, C. Thomsen, R. Liu, H. G. von Schnering, M. Hartweg, Y. F. Yan, and Z. X. Zhao, Solid State Commun. **66** 1255 (1988).

[46] R. Liu, M. V. Klein, P. D. Han, and D. A. Payne, Phys. Rev. B **45** 7392 (1992).

[47] M. Boekholt, A. Erle, P. C. Splittgerber-Hunnekes, and G. Guntherodt, Solid State Commun. **74** 1107 (1990).

[48] M. Kakihana, M. Osada, M. Käll, L. Börjesson, H. Mazaki, H. Yasuoka, M. Yashima, M. Yoshimura, Phys. Rev. B **53** 11796 (1996).

[49] A. E. Pantoya, D. M. Pooke, H. J. Trodahl, J. C. Irwin, Phys. Rev. B **58** 5219 (1998).

[50] L. Ben-Dor, M. Y. Szerer, G. Blumberg, A. Givan, L. Börjesson, and L. V. Hong, Physica C **200** 418 (1992).

[51] V. G. Hadjiev, Xingjiang Zhou, T. Strohm, M. Cardona, Q. M. Lin, C. W. Chu, Phys. Rev. B **58** 1043 (1998).

[52] Michail Limonov, Sergey Lee, and Setsuko Tajima, Phys. Rev. B **66** 054509 (2002).

[53] D. Munzar and M. Cardona, Phys. Rev. Lett. **90** 077001 (2003).

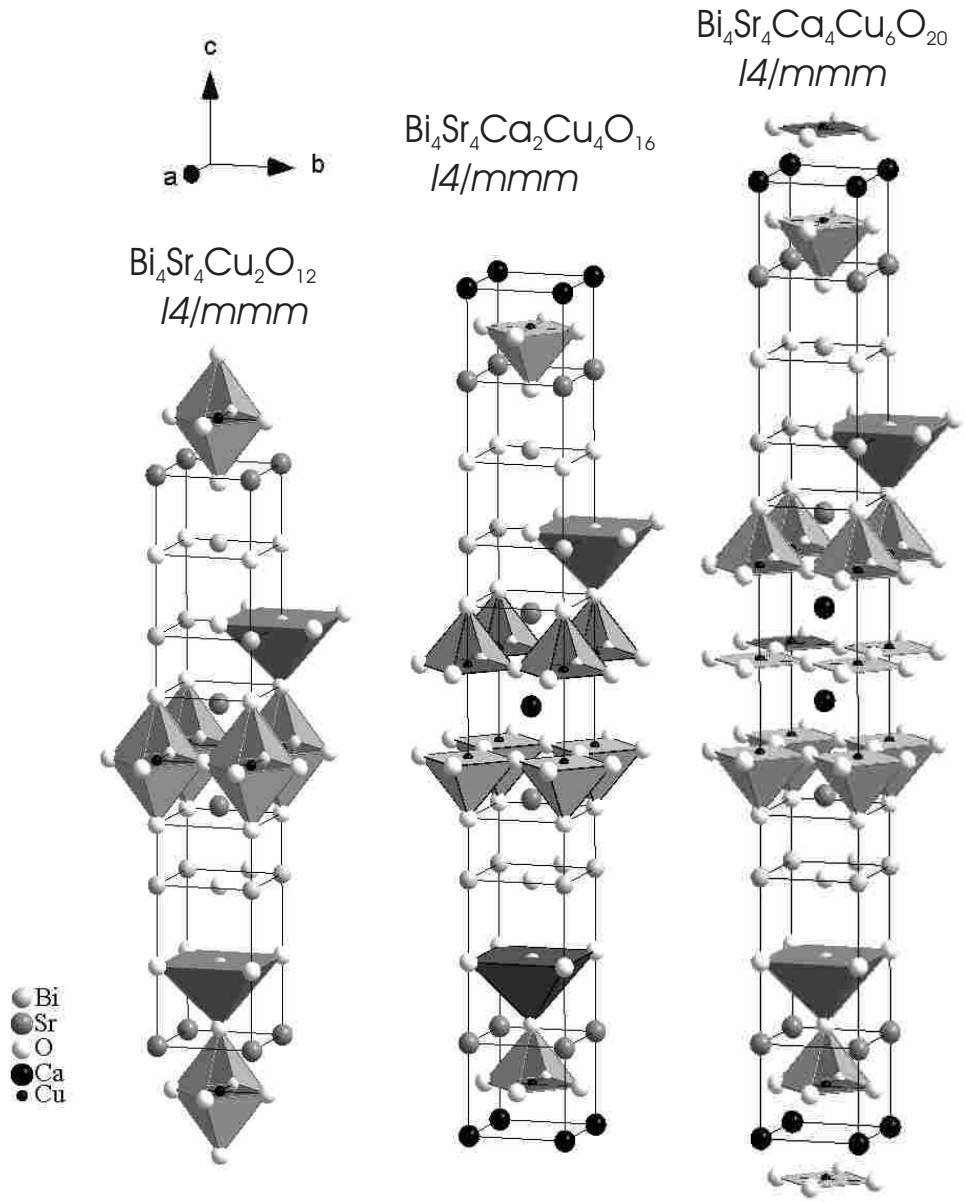


FIG. 1: Crystallographic cells of $Bi_2Sr_2Ca_{n-1}Cu_nO_{2n+4}$ with n = 1, 2 and 3.

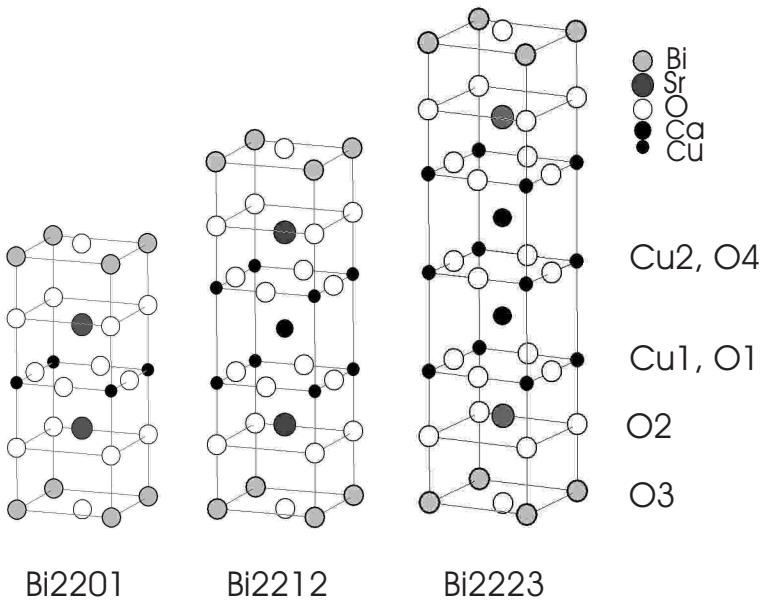


FIG. 2: Notations for copper and oxygen atoms in primitive unit cells of single, bi-, and trilayer Bi-based cuprates.

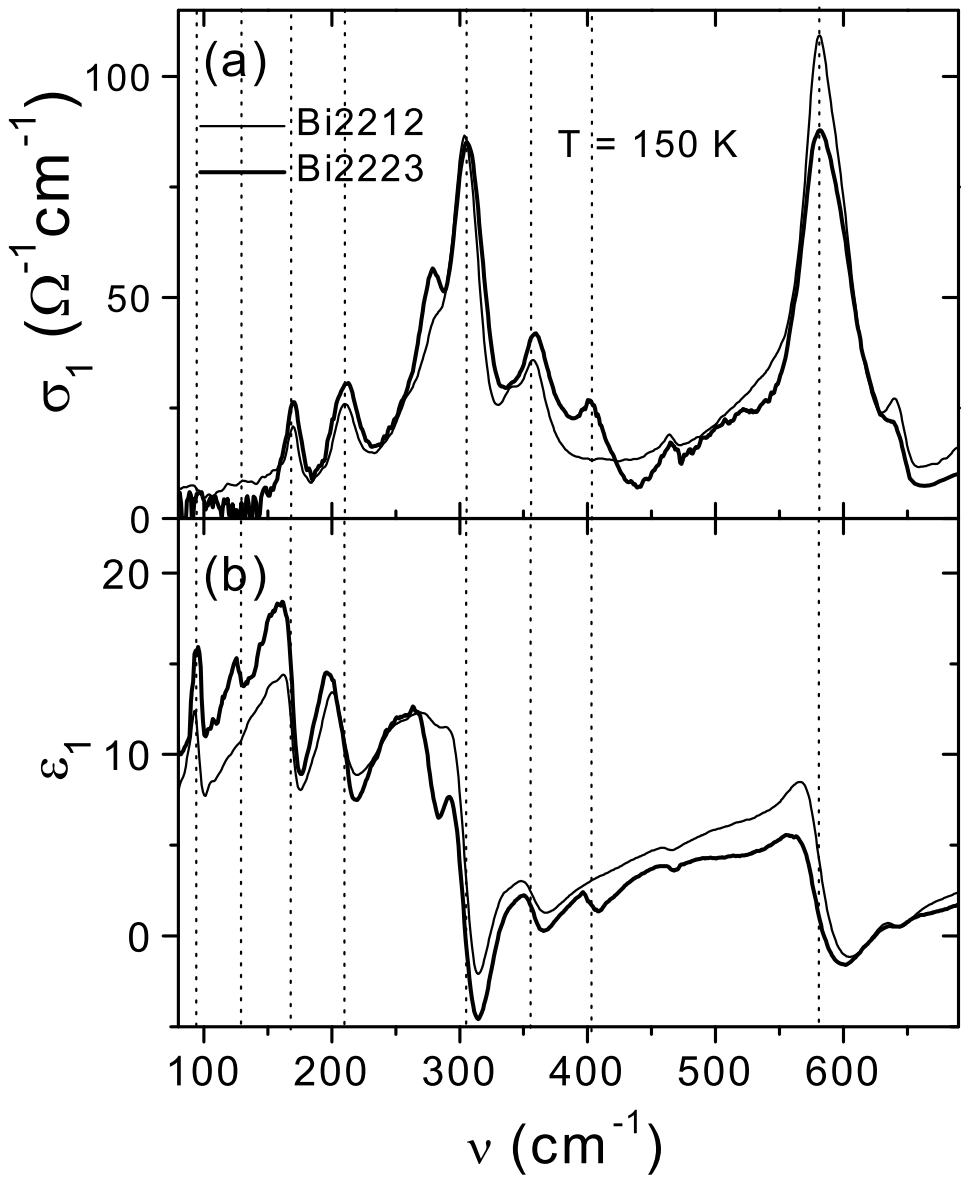


FIG. 3: Real parts of the c axis (a) optical conductivity $\sigma_1(\omega)$ and (b) dielectric function $\epsilon_1(\omega)$ of Bi2212 and Bi2223 single crystals with $T_c = 91$ K and $T_c = 107$ K at T = 150 K.

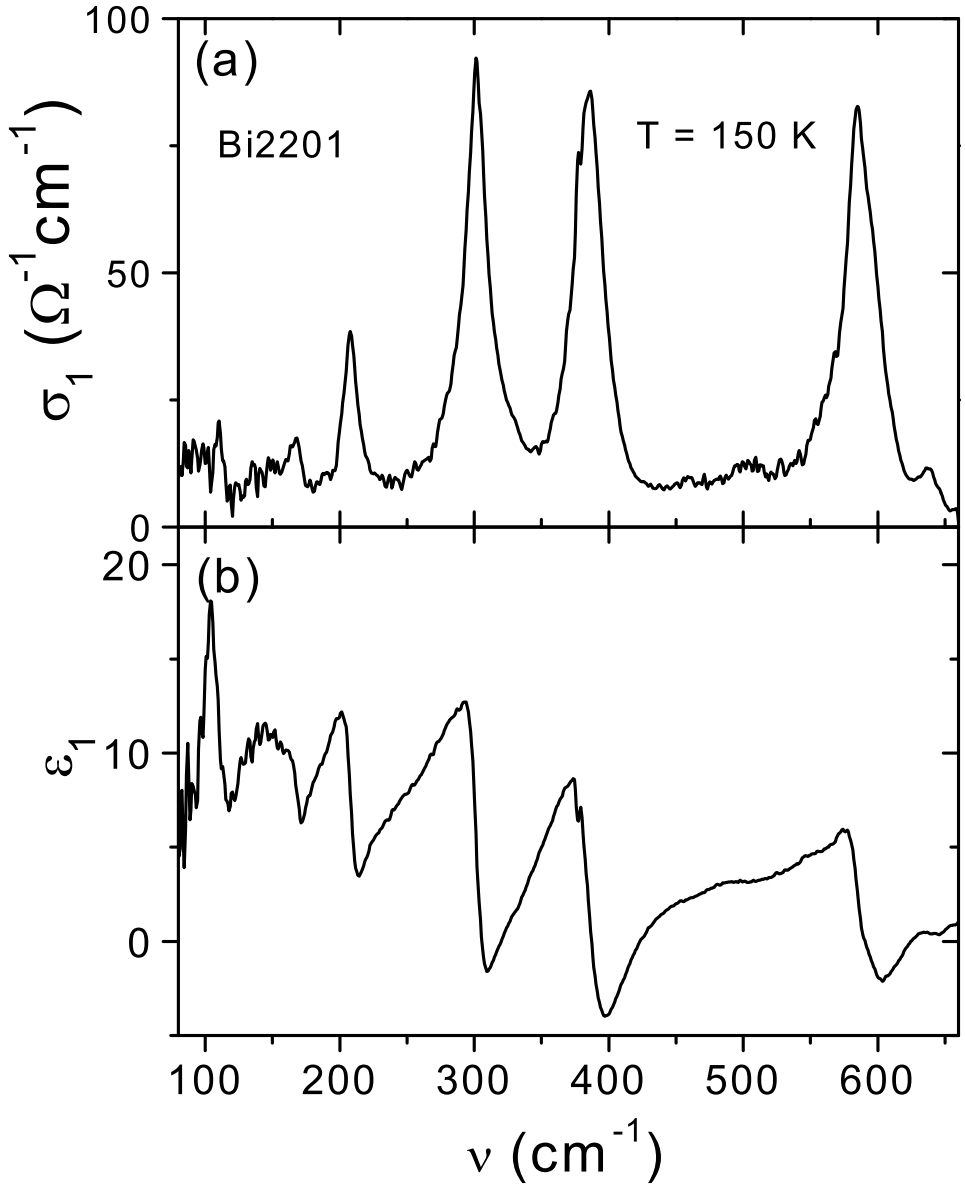


FIG. 4: C axis (a) optical conductivity $\sigma_1(\omega)$ and (b) dielectric function $\epsilon_1(\omega)$ of Bi2201 single crystal at T = 150 K.

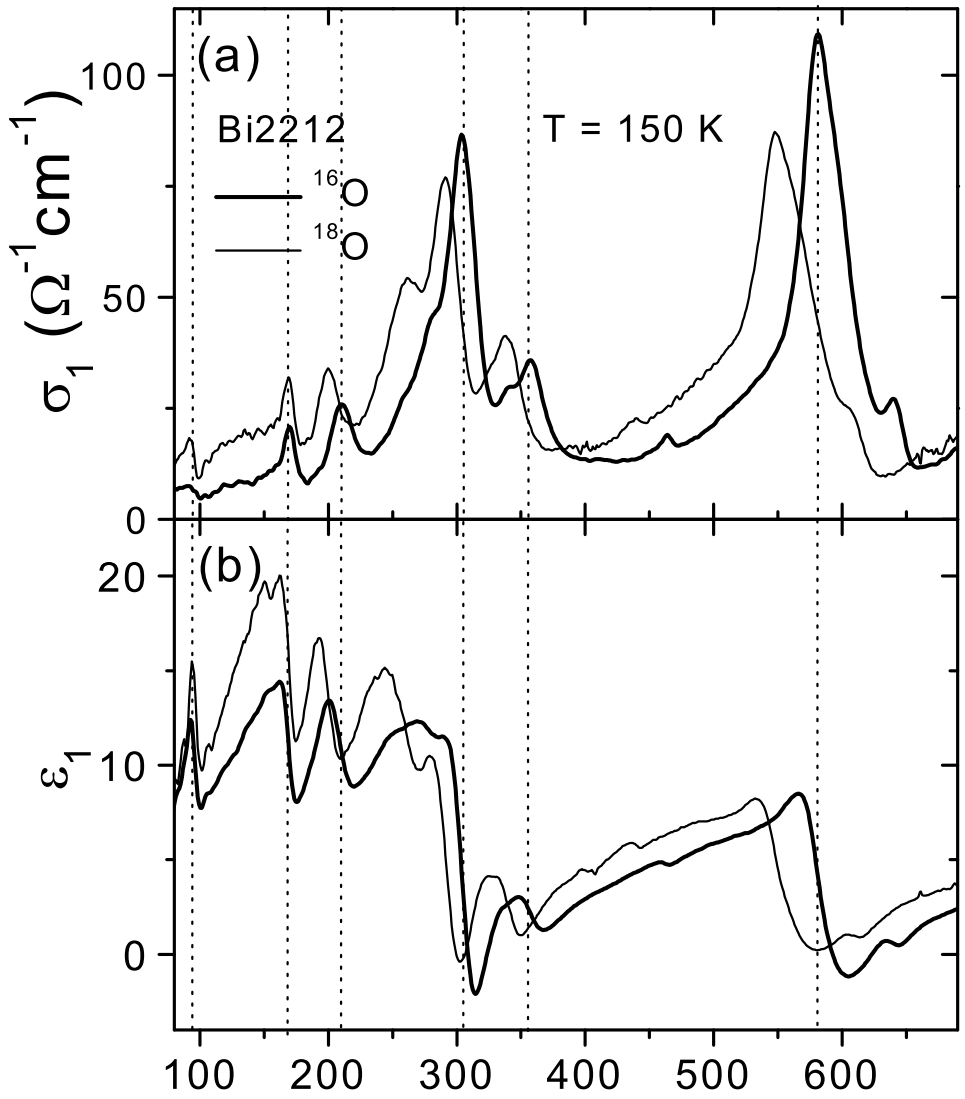


FIG. 5: Oxygen isotope effect in the c-polarized response of (a) $\sigma_1(\omega)$ and (b) $\epsilon_1(\omega)$ of Bi2212 with $T_c = 91$ K, measured at 150 K.

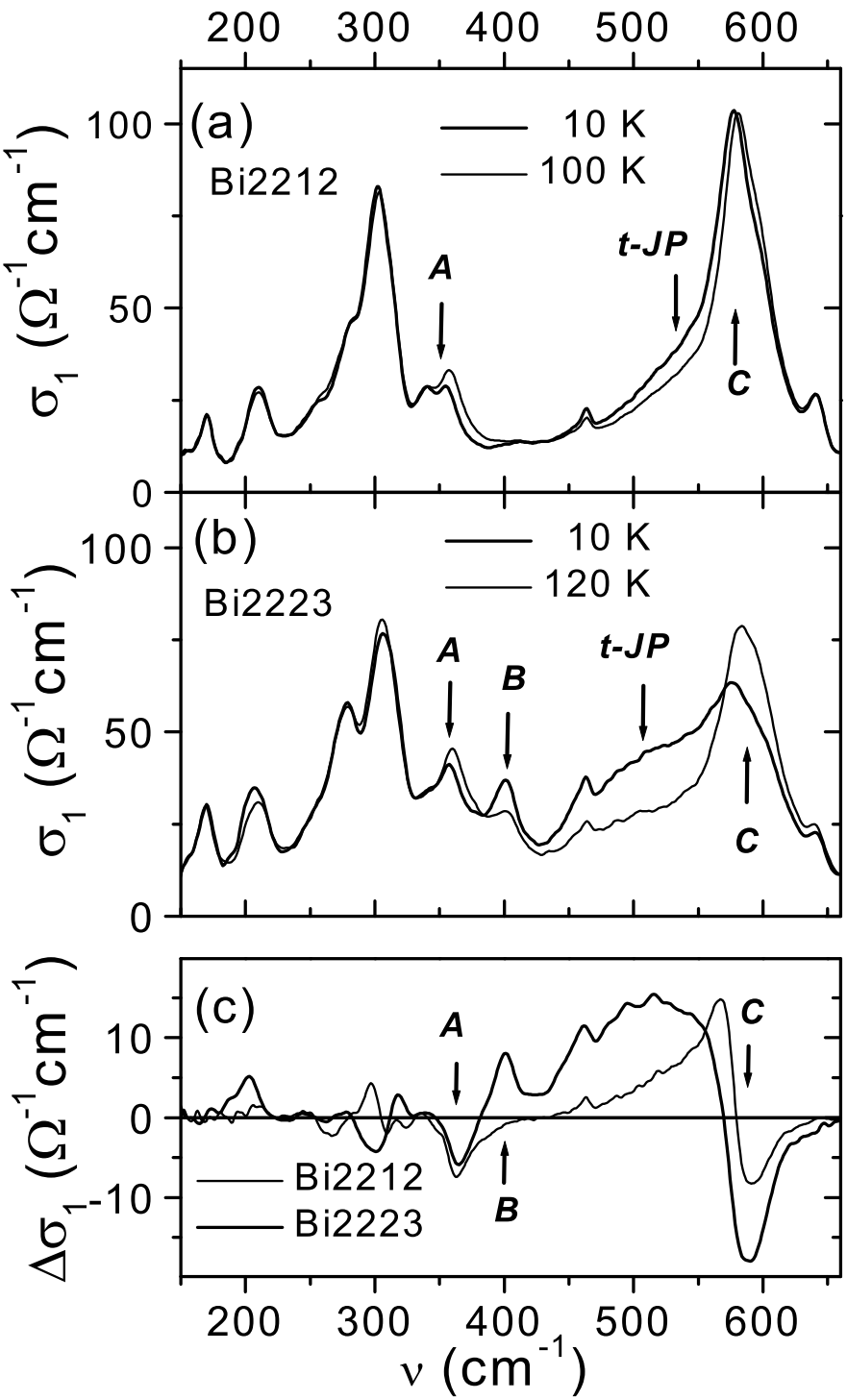


FIG. 6: Real part $\sigma_1(\omega)$ of the FIR c axis conductivity (a) of Bi2212 with $T_c = 91$ K for $T = 100$ K and $T = 10$ K [6] and (b) of Bi2223 with $T_c = 102$ K for $T = 120$ K and $T = 10$ K [7]. (c) Superconductivity-induced changes of the FIR conductivity, $\Delta\sigma_1 = \sigma_1(T << T_c, \omega) - \sigma_1(T \gtrsim T_c, \omega)$, for Bi2212 and Bi2223 derived from the data shown in the top panels. The most pronounced phonon anomalies are denoted by A, B, and C.

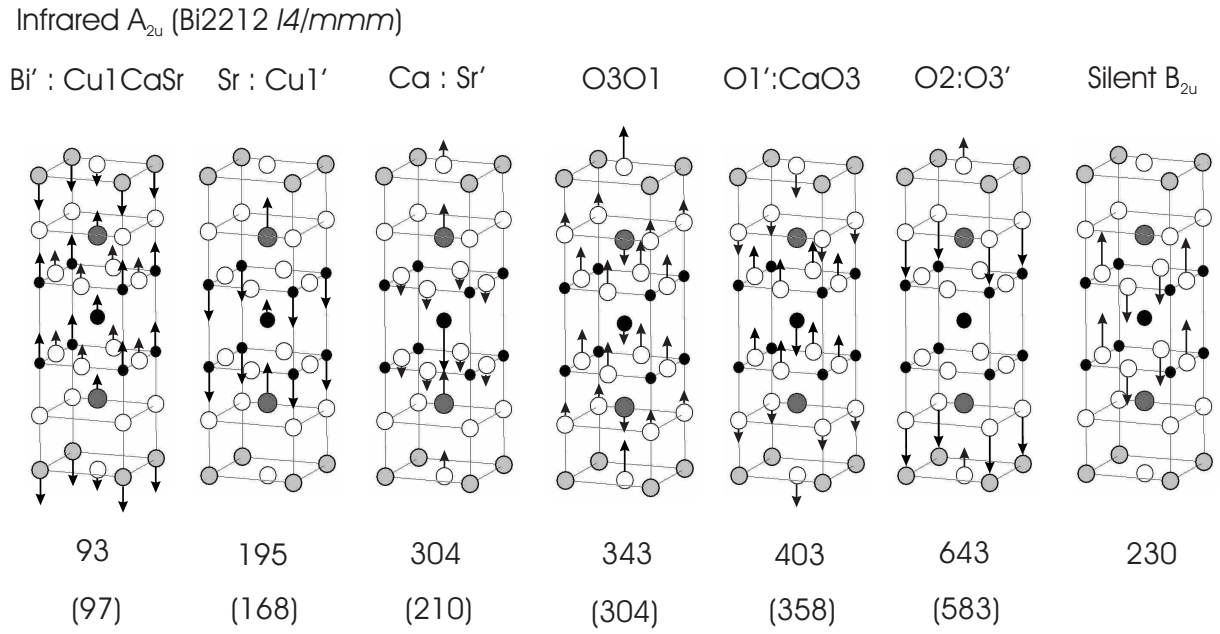


FIG. 7: Normal frequencies (in cm^{-1}) of six A_{2u} symmetry modes and one "silent" B_{2u} mode in Bi2212 ($I4/mmm$) and schematic representation of their eigenvectors; respective experimental c axis TO phonon frequencies are given in brackets (see Figure 3 and Table 6).

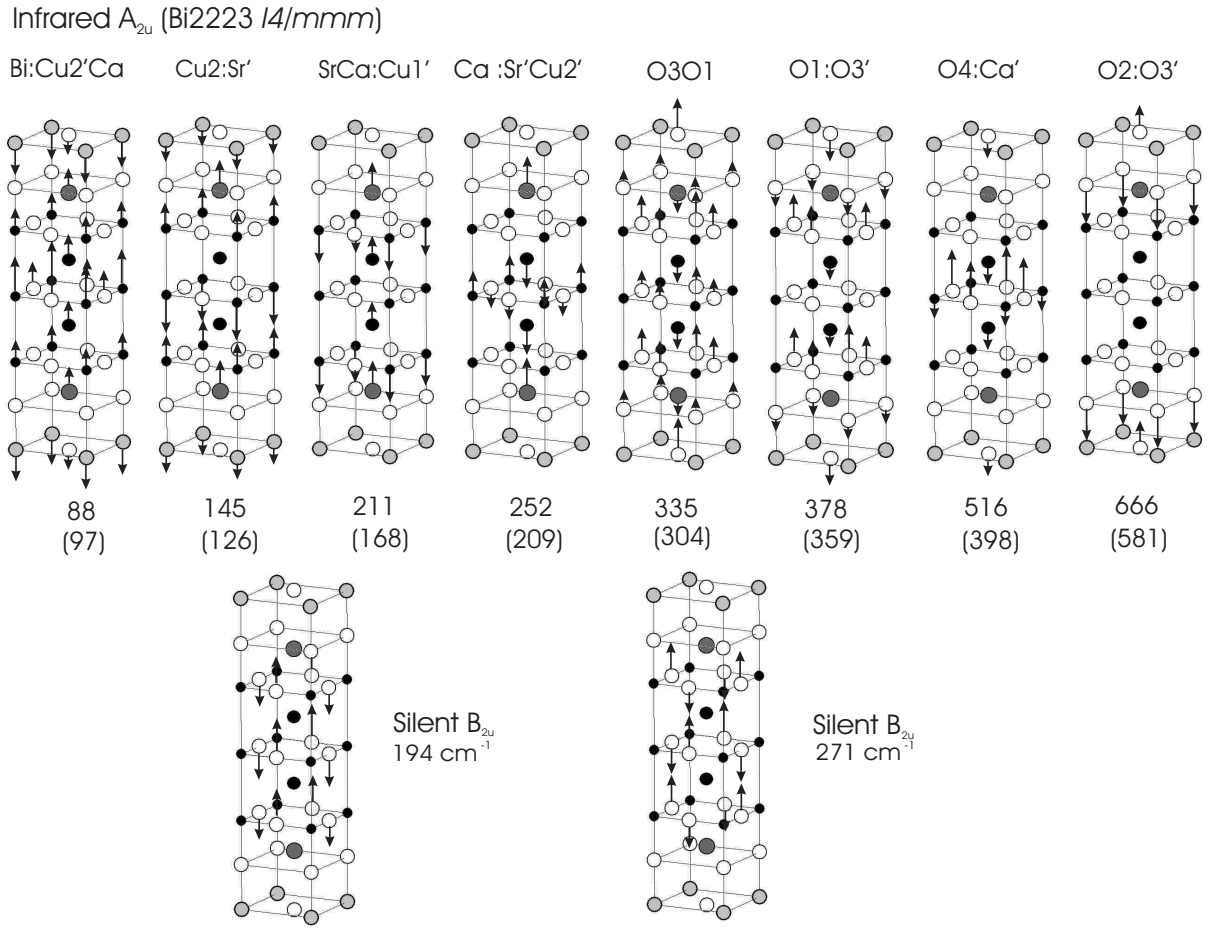


FIG. 8: Normal frequencies and eigenvectors of eight A_{2u} symmetry modes and two "silent" B_{2u} modes in Bi2223 ($I4/mmm$); respective experimental c axis TO phonon frequencies are given in brackets (see Figure 3 and Table 6).

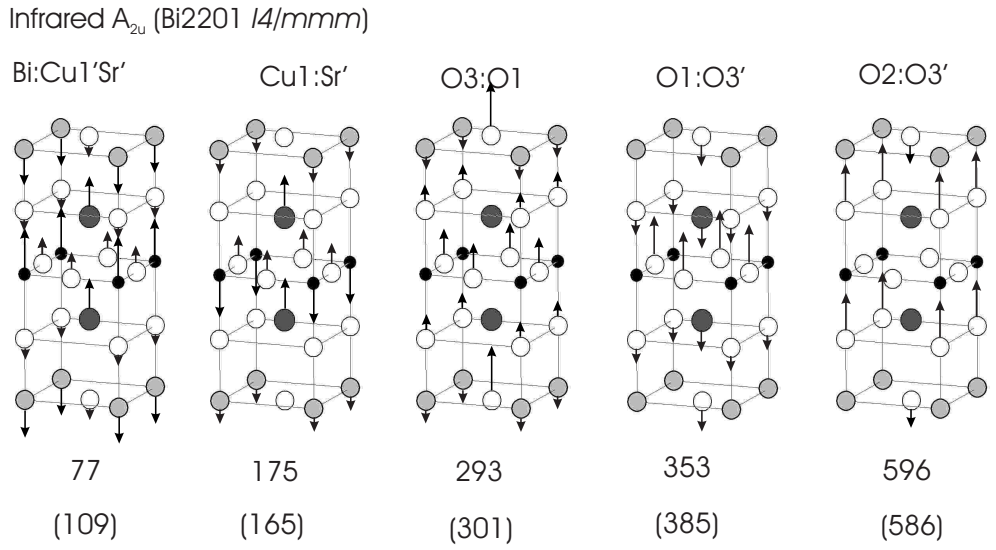


FIG. 9: Normal frequencies and eigenvectors of five A_{2u} symmetry modes in Bi2201 ($I4/mmm$); experimental c axis TO phonon frequencies are given in brackets (see Figure 4 and Table 6).

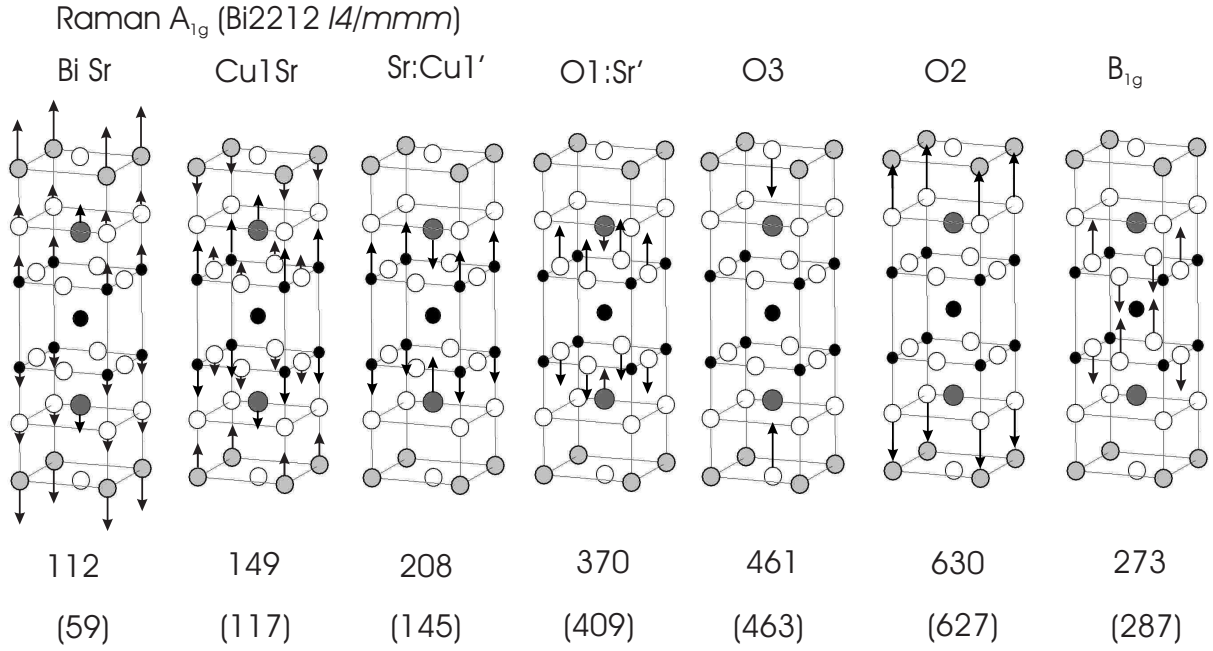


FIG. 10: Normal frequencies and eigenvectors of six A_{1g} symmetry modes and one B_{1g} mode in Bi2212 ($I4/mmm$); experimental frequencies are given in brackets [48].

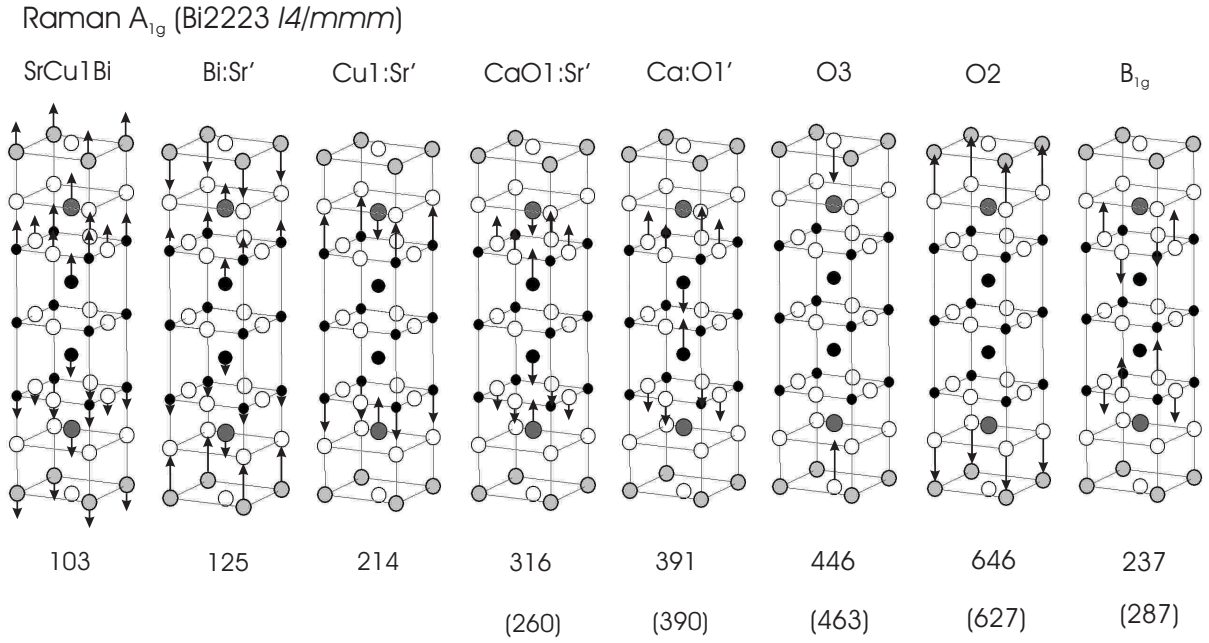


FIG. 11: Normal frequencies and eigenvectors of seven A_{1g} symmetry modes and one B_{1g} mode in Bi2223 ($I4/mmm$); some of experimental frequencies are given in brackets (see Figure 13 and Ref. [52]).

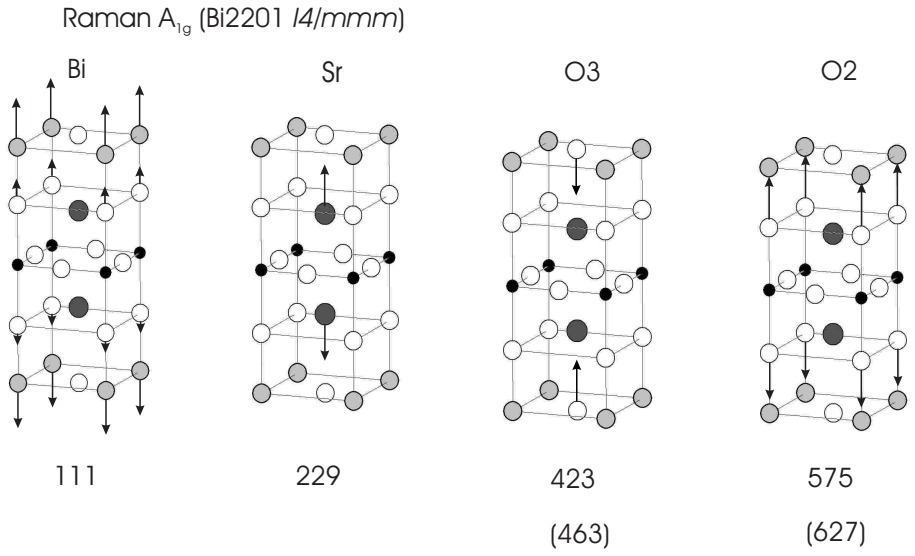


FIG. 12: Normal frequencies and eigenvectors of four A_{1g} symmetry modes in Bi2201 ($I4/mmm$); some of the experimental frequencies are given in brackets [48].

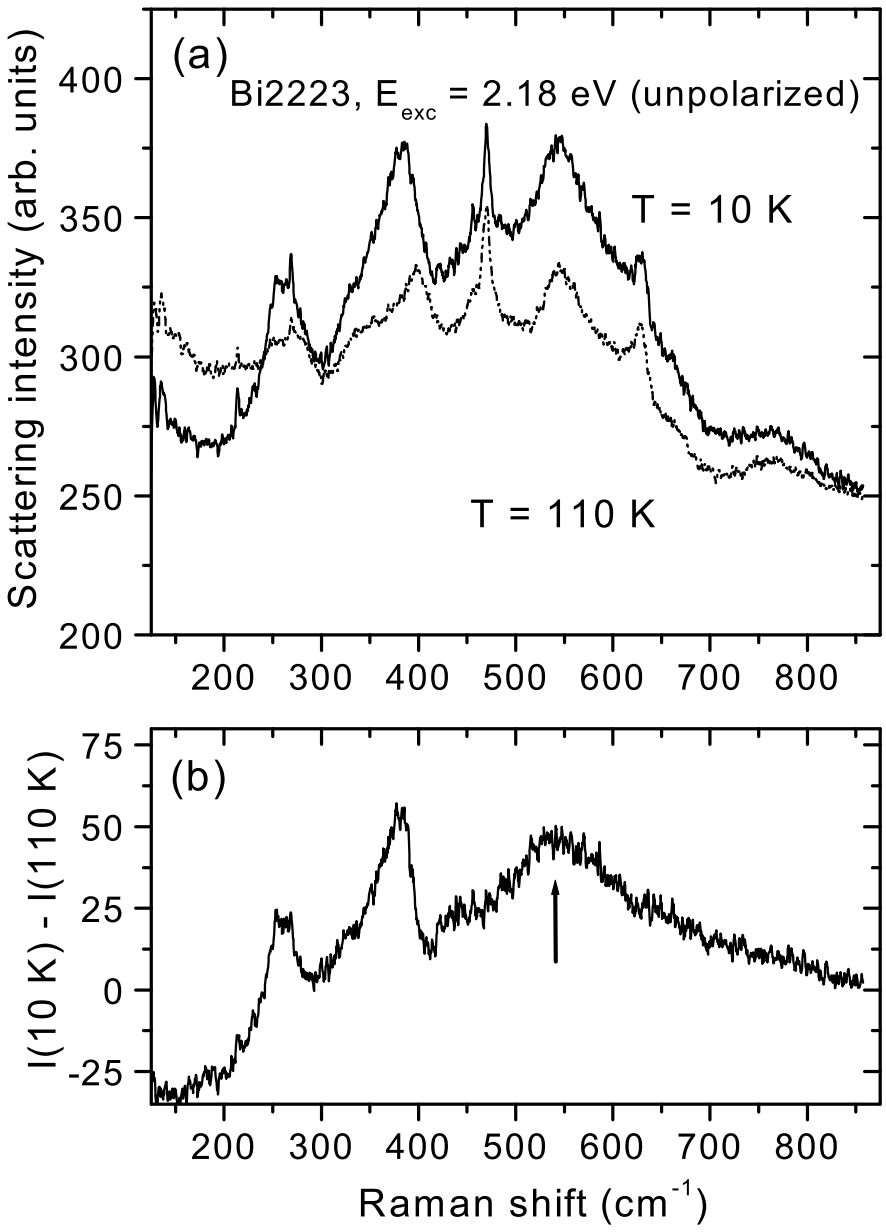


FIG. 13: Raman scattering (E_{exc} = 2.18 eV) in Bi2223 (a) measured slightly above T_c = 107 K and well below T_c and (b) resonant enhancement of the phonon bands at 260 and 390 cm^{-1} and superconductivity-induced broad band at 550 cm^{-1}.